

# An Effective Model of the Retinoic Acid Induced HL-60 Differentiation Program

Ryan Tasseff, Holly A. Jensen, Johanna Congleton<sup>†</sup>, Wei Dai, Katherine Rogers, Adithya Sagar, Rodica P. Bunaciu<sup>†</sup>, Andrew Yen<sup>†</sup>, and Jeffrey D. Varner\*

Robert Frederick Smith School of Chemical and Biomolecular Engineering and <sup>†</sup>Department of Biomedical Sciences, Cornell University, Ithaca NY 14853

**Running Title:** Effective modeling of HL-60 differentiation

**To be submitted:** *Oncotarget*

\*Corresponding author:

Jeffrey D. Varner,

Professor, Robert Frederick Smith School of Chemical and Biomolecular Engineering,  
244 Olin Hall, Cornell University, Ithaca NY, 14853

Email: jdv27@cornell.edu

Phone: (607) 255 - 4258

Fax: (607) 255 - 9166

## Abstract

In this study, we present an effective model All-Trans Retinoic Acid (ATRA)-induced differentiation of HL-60 cells. The model describes a key architectural feature of ATRA-induced differentiation, reinforcing feedback between an ATRA-inducible signalsome complex involving many proteins including Vav1, a guanine nucleotide exchange factor, and the activation of the mitogen activated protein kinase (MAPK) cascade. We decomposed the effective model into three modules; a signal initiation module that sensed and transformed an ATRA signal into program activation signals; a signal integration module that controlled the expression of upstream transcription factors; and a phenotype module which encoded the expression of functional differentiation markers from the ATRA-inducible transcription factors. The model, which was developed by integrating logical rules with kinetic modeling, was significantly smaller than previous models. However, despite its simplicity, it captured key features of ATRA induced differentiation of HL-60 cells. We identified an ensemble of effective model parameters using measurements taken from ATRA-induced HL-60 cells. Using these parameters, model analysis predicted that MAPK activation was bistable as a function of ATRA exposure. Conformational experiments supported ATRA-induced bistability. Additionally, the model captured intermediate and phenotypic gene expression data. Knockout analysis suggested Gfi-1 and PPAR $\gamma$  were critical to the ATRA-induced differentiation program. These findings, combined with other literature evidence, suggested that reinforcing feedback is central to hyperactive signaling in a diversity of cell fate programs.

## **1 Introduction**

2 Differentiation induction chemotherapy (DIC), using agents such as the vitamin A derivative  
3 all-trans retinoic acid (ATRA), is a promising approach for the treatment of many cancers (1–5). For example, ATRA treatment induces remission in 80–90% of promyelocytic  
4 leukemia (APL) PML-RAR $\alpha$ -positive patients (6), thereby transforming a fatal diagnosis  
5 into a manageable disease (7). However, remission is sometimes not durable and re-  
6 lapsed cases exhibit emergent ATRA resistance (8, 9). To understand the basis of this re-  
7 sistance, we must first understand the ATRA-induced differentiation program. Toward this  
8 challenge, lessons learned in model systems, such as the lineage-uncommitted human  
9 myeloblastic cell line HL-60 reported to closely resemble patient derived cells (10), could  
10 inform our analysis of the differentiation programs occurring in patients. Patient derived  
11 HL-60 leukemia cells have been a durable experimental model since the 1970's to study  
12 differentiation (11). HL-60 undergoes cell cycle arrest and either myeloid or monocytic  
13 differentiation following stimulation; ATRA induces G1/G0-arrest and myeloid differentia-  
14 tion in HL-60 cells, while 1,25-dihydroxy vitamin D3 (D3) induces arrest and monocytic  
15 differentiation. Commitment to cell cycle arrest and differentiation requires approximately  
16 48 hr of treatment, during which HL-60 cells undergo two division cycles.

18 Sustained mitogen-activated protein kinase (MAPK) pathway activation is a defining  
19 feature of ATRA-induced HL-60 differentiation. ATRA drives sustained activation of the  
20 Raf/MEK/ERK pathway, leading to arrest and differentiation (12). Betraying a feedback  
21 loop, MEK inhibition results in the loss of ERK as well as Raf phosphorylation and the  
22 failure to arrest and differentiate in response to ATRA (13). Retinoic acid (and its metabo-  
23 lites) are ligands for the hormone activated nuclear transcription factors retinoic acid re-  
24 ceptor (RAR) and retinoid X receptor (RXR) (14). RAR/RXR activation is necessary for  
25 ATRA-induced Raf phosphorylation (13) in concert with the formation of an ATRA-induced  
26 signalsome complex at the membrane, which drives MAPK activation. While the makeup

27 of the signalsome complex is not yet known, we do know that it is composed of Src  
28 family kinases Fgr and Lyn, PI3K, c-Cbl, Slp76, and KSR, plus transcription factors AhR  
29 and IRF1 (15–19). Signalsome activity is driven by ATRA-induced expression of CD38  
30 and putatively the heterotrimeric Gq protein-coupled receptor BLR1 (20, 21). BLR1 (also  
31 known as CXCR5), identified as an early ATRA (or D3)-inducible gene using differential  
32 display (22), is necessary for MAPK activation and differentiation (21), and drives sig-  
33 nalsome activity. Studies of the BLR1 promoter identified a non-canonical RARE site  
34 consisting of a 17 bp GT box approximately 1 kb upstream of the transcriptional start  
35 that conferred ATRA responsiveness (21). Members of the BLR1 transcriptional activator  
36 complex, e.g. NFATc3 and CREB, are phosphorylated by ERK, JNK or p38 MAPK fam-  
37 ily members suggesting positive feedback between the signalsome and MAPK activation  
38 (23, 24). BLR1 overexpression enhanced Raf phosphorylation and accelerated terminal  
39 differentiation, while Raf inhibition reduced BLR1 expression and ATRA-induced terminal  
40 differentiation (25). In particular, Raf phosphorylation of the NFATc3 transcription factors  
41 at the BLR1 promoter enables transcriptional activation at the RARE by ATRA bound to  
42 RAR/RXR (26). BLR1 knock-out cells failed to activate Raf or differentiate in the pres-  
43 ence of ATRA (25). Interestingly, both the knockdown or inhibition of Raf, also reduced  
44 BLR1 expression and functional differentiation (25). Thus, the expression of signalsome  
45 components e.g., BLR1 was Raf dependent, while Raf activation depended upon the sig-  
46 nalsome. A previous computational study of ATRA-induced differentiation of HL-60 cells  
47 suggested that the BLR1-MAPK positive feedback circuit was sufficient to explain ATRA-  
48 induced sustained MAPK activation, and the expression of a limited number of functional  
49 differentiation markers (27). Model analysis also suggested that Raf was the most distinct  
50 of the MAPK proteins. However, this previous study developed and analyzed a complex  
51 model, thus leaving open the critical question of what is the minimal positive feedback  
52 circuit required to drive ATRA-induced differentiation.

53 In this study, we explored this question using a minimal mathematical model of the  
54 key architectural feature of ATRA induced differentiation of HL-60 cells, namely positive  
55 feedback between an ATRA-inducible signalsome complex and MAPK activation. The  
56 ATRA responsive signalsome-MAPK circuit was then used to drive a downstream gene  
57 expression program which encoded for the expression of intermediate and functional dif-  
58 ferentiation markers. The effective model used a novel framework which integrated logi-  
59 cal rules with kinetic modeling to describe gene expression and protein regulation, while  
60 largely relying upon biophysical parameters from the literature. This formulation signif-  
61 icantly reduced the size and complexity of the model compared to the previous study  
62 of Tasseff et al., while increasing the breadth of the biology described (27). The effec-  
63 tive model, despite its simplicity, captured key features of ATRA induced differentiation  
64 of HL-60 cells. Model analysis predicted the bistability of MAPK activation as a func-  
65 tion of ATRA exposure; conformational experiments supported ATRA-induced bistability.  
66 Model simulations were also consistent with measurements of the influence of MAPK in-  
67 hibitors, and the failure of BLR1 knockout cells to differentiate when exposed to ATRA.  
68 In addition, the expression of intermediate and phenotypic differentiation markers as also  
69 captured following ATRA exposure. Lastly, we showed through immunoprecipitation and  
70 inhibitor studies, that the guanine nucleotide exchange factor Vav1 is potentially a new  
71 ATRA-inducible member of the signalsome complex functioning as a regulator that con-  
72 tributes to signal amplification in the signalsome. Taken together, these findings when  
73 combined with other literature evidence, suggested that reinforcing feedback was central  
74 to differentiation programs generally, and necessary for ATRA-induced differentiation. The  
75 model answers a biologically important question that is not easily experimentally attacked,  
76 namely given the complexity of the signaling machine and the pathways it embodies, is  
77 there a critical small suite of molecules that are the action elements seminal to eliciting  
78 ATRA-induced cell differentiation and G0 arrest.

79 **Results**

80 We constructed an effective model of ATRA-induced HL-60 differentiation which described  
81 signaling and gene expression events following the addition of ATRA (Fig. 1). The model  
82 connectivity was developed from literature and the studies presented here (Table 1). We  
83 decomposed the ATRA program into three modules; a signal initiation module that sensed  
84 and transformed the ATRA signal into activated cRaf-pS621 and the ATRA-RAR/RXR  
85 (Trigger) signals (Fig. 1A); a signal integration module that controlled the expression  
86 of upstream transcription factors given cRaf-pS621 and activated Trigger signals (Fig.  
87 1B); and a phenotype module which encoded the expression of functional differentiation  
88 markers from the ATRA-inducible transcription factors (Fig. 1C). In particular, Trigger (a  
89 surrogate for the RAR $\alpha$ /RXR transcriptional complex) regulated the expression of the tran-  
90 scription factors CCATT/enhancer binding protein  $\alpha$  (C/EBP $\alpha$ ), PU.1, and Egr-1. In turn,  
91 these transcription factors, in combination with cRaf-pS621, regulated the expression of  
92 downstream phenotypic markers such as CD38, CD11b or p47Phox. Each component of  
93 these modules was described by a mRNA and protein balance equation. Additionally, the  
94 signal initiation module also described the abundance of activated species e.g., Trigger  
95 and cRaf-pS621 whose values were derived from unactivated Trigger and cRaf protein  
96 levels. Lastly, because the population of HL-60 cells was dividing, we also considered  
97 a dilution term in all balance equations. The signal initiation module contained nine dif-  
98 ferential equations, while the signal integration and phenotype modules were collectively  
99 encoded by 54 differential equations. Model parameters were taken from literature (Table  
100 2), or estimated from experimental data using heuristic optimization (see materials and  
101 methods).

102 The signal initiation module recapitulated sustained signalsome and MAPK activation  
103 following exposure to 1 $\mu$ M ATRA (Fig. 2A-B). An ensemble of effective model param-  
104 eters was estimated by minimizing the difference between simulations and time-series

105 measurements of BLR1 mRNA and cRaf-pS621 following the addition of  $1\mu\text{M}$  ATRA. We  
106 focused on the S621 phosphorylation site of cRaf since enhanced phosphorylation at this  
107 site is a defining characteristic of sustained MAPK signaling activation in HL-60. The  
108 effective model captured both ATRA-induced BLR1 expression (Fig. 2A) and sustained  
109 phosphorylation of cRaf-pS621 (Fig. 2B) in a growing population of HL-60 cells. To-  
110 gether, the reinforcing feedback within the signalsome and its embedded MAPK signaling  
111 axis led to sustained activation over multiple cellular generations. However, the effective  
112 model failed to capture the decline of BLR1 message after 48 hr of ATRA exposure. This  
113 suggested that we captured the logic leading to the onset of differentiation, but failed to  
114 describe program shutdown. Much of the focus in the literature has been on understand-  
115 ing the initiation of differentiation, with little attention paid to understanding how a program  
116 is terminated. This is a potential new direction that could be explored. Next, we tested  
117 the response of the signal initiation module to different ATRA dosages.

118 The signal initiation model was bistable with respect to ATRA induction (Fig. 2C-D).  
119 Phaseplane analysis predicted two stable steady-states when ATRA was present below  
120 a critical threshold (Fig. 2C), and only a single steady-state above the threshold (Fig.  
121 2D). In the lower stable state, neither the signalsome nor cRaf-pS621 were present (thus,  
122 the differentiation program was inactive). However, at the higher stable state, both the  
123 signalsome and cRaf-pS621 were present, allowing for sustained activation and differen-  
124 tiation. Interestingly, when ATRA was above a critical threshold, only the activated state  
125 was accessible (Fig. 2D). To test these findings, we first identified the ATRA threshold. We  
126 exposed HL-60 cells to different ATRA concentrations for 72 hr (Fig. 2E). Morphological  
127 changes associated with differentiation were visible for  $\text{ATRA} \geq 0.25\mu\text{M}$ , suggesting the  
128 critical ATRA threshold was near this concentration. Next, we conducted ATRA washout  
129 experiments to determine if activated cells remained activated in the absence of ATRA.  
130 HL-60 cells locked into an activated state remained activated following ATRA withdraw

(Fig. 3C). This sustained activation resulted from reinforcing feedback between the signalsome and the MAPK pathway. Thus, following activation, if we inhibited or removed elements from the signal initiation module we expected the signalsome and MAPK signals to decay. We simulated ATRA induced activation in the presence of kinase inhibitors, and without key circuit elements. Consistent with experimental results using multiple MAPK inhibitors, ATRA activation in the presence of MAPK inhibitors lowered the steady-state value of signalsome (Fig. 3A). In the presence of BLR1, the signalsome and cRaf-pS621 signals were maintained following ATRA withdraw (Fig. 3B, gray). On the other hand, BLR1 deletion removed the ability of the circuit to maintain a sustained MAPK response following the withdraw of ATRA (Fig. 3B, blue). Lastly, washout experiments in which cells were exposed to  $1\mu\text{M}$  ATRA for 24 hr, and then transferred to fresh media without ATRA, confirmed the persistence of the self sustaining activated state for up to 144 hr (Fig. 3C). Thus, these experiments confirmed that reinforcing positive feedback likely drives the ATRA-induced differentiation program. Next, we analyzed the ATRA-induced downstream gene expression program following signalsome and cRaf activation.

The signal integration and phenotype modules described ATRA-induced gene expression in wild-type HL-60 cells (Fig. 4). The signal initiation module produced two outputs, activated Trigger and cRaf-pS621 which drove the expression of ATRA-induced transcription factors, which then in turn activated the phenotypic program. We assembled the connectivity of the signal integration and phenotypic programs driven by Trigger and cRaf-pS621 from literature (Table 1). We estimated the parameters for the signal initiation, and phenotype modules from steady-state and dynamic measurements of transcription factor and phenotypic marker expression following the addition of ATRA (28–31). However, the bulk of the model parameters were taken from literature (32) and were not estimated in this study (see materials and methods). The model simulations captured the time dependent expression of CD38 and CD11b following the addition ATRA (Fig. 4A), and the

157 steady-state for signal integration and phenotypic markers (Fig. 4B). Lastly, we used the  
158 *predicted* values of the p21 and E2F protein abundance to estimate a blackbox model of  
159 ATRA-induced G0 arrest (Fig. 5). The phenotype module predicted p21 expression sig-  
160 nificantly increased and E2F expression decreased, in response to ATRA exposure (Fig.  
161 5A). We then used the ratio of these values in a polynomial model to calculate the frac-  
162 tion of HL-60 cells in G0 arrest following the addition of ATRA (Fig. 5B). The third-order  
163 polynomial model captured the trend in measured G0-arrest values as a function of time,  
164 and was robust to uncertainty in the measured data (Fig. 5B, gray). Taken together, the  
165 output of the signal integration and phenotypic modules was consistent with time-series  
166 and steady-state measurements, thereby validating the assumed molecular connectivity.  
167 Moreover, outputs from the phenotype module described the trend in ATRA-induced G0  
168 cell cycle arrest. Next, we explored which proteins and protein interactions in the signal  
169 integration module most influenced the system response.

170 The Gfi-1 and PPAR $\gamma$  proteins were important regulators of ATRA-induced signal in-  
171 tegration and phenotypic change (Fig. 6). We conducted pairwise gene knockout simu-  
172 lations in the signal integration and phenotype modules to estimate which proteins con-  
173 trolled the processing of the Trigger and cRaf-S621 signals. The difference between the  
174 system state with and without the gene knockouts (encoded as a normalized state dis-  
175 placement matrix) was decomposed using Singular Value Decomposition (SVD). A panel  
176 of ten parameter sets was sampled, and the average normalized displacement matrix  
177 was decomposed. The first six modes (approximately 36% of the total) described >95%  
178 of the gene knockout variance, with the most important components of these modes be-  
179 ing the Gfi-1 and PPAR $\gamma$  proteins, and to a lesser extent PU.1, C/EBP $\alpha$  and AP1  
180 (Fig. 6A). To better understand which protein-DNA connections were important, we sim-  
181 ulated the pairwise deletion of interactions between these proteins and their respective  
182 regulatory targets. Singular value decomposition of the normalized state displacement

matrix assembled from the pairwise connection deletions, suggested the first six modes (approximately 26% of the total) accounted for >90% of the variance. Globally, the most sensitive interactions controlled p21 and p47Phox expression, markers for cell-cycle arrest and reactive oxygen formation phenotypic axes activated following ATRA addition (Fig. 6B). Analysis of the modes suggested the action of PPAR $\gamma$ , Gfi-1 and C/EBP $\alpha$  were consistently important over multiple target genes. The connection knockout analysis also revealed robustness in the network. For example, no pair of deletions qualitatively changed the expression of regulators such as PU.1, Oct1, Oct4 or PPAR $\gamma$ . Thus, the expression of these species was robust to disturbance in the connectivity. To better understand the combined influence of the PPAR $\gamma$  and Gfi-1 deletions, we computed the fold change in the protein levels in the single (Gfi-1 $^{-/-}$  or PPAR $\gamma$  $^{-/-}$ ) and double (Gfi-1 $^{-/-}$  and PPAR $\gamma$  $^{-/-}$ ) mutants for the best fit parameter set (Fig. 7). Deletion of Gfi-1 led to a 2-4 fold increase in EGR-1, CD11b and C/EBP $\alpha$  expression, and a >8 fold increase in PU.1 abundance (Fig. 7,blue). On the other hand, deletion of PPAR $\gamma$  led to >8 fold down-regulation of CD38, p21, IRF1 and Oct1 (Fig. 7,red). Both knockouts slightly increased E2F expression, but neither influenced the expression of p47Phox. The double mutant was qualitatively similar to the combined behavior of the two single mutant cases. Taken together, Gfi-1 and PPAR $\gamma$  controlled the cell-cycle arrest and receptor signaling axes, with PPAR $\gamma$  regulating CD38, IRF1 and p21 expression while Gfi-1 controlled CD11b expression. These simulations suggested deletion of PPAR $\gamma$  and Gfi-1 would not interfere with reactive oxygen formation, but would limit the ability of HL-60 cells to arrest. However, this analysis did not give insight into which components upstream of the signal initiation module were important. Toward this question, we explored the composition and regulation of the signalsome complex by experimentally interrogating a panel of possible Raf interaction partners.

The full composition of the signalsome, and the kinase therein ultimately responsible

for mediating ATRA-induced Raf activation is still not known. To explore this question, we conducted immunoprecipitation and subsequent Western blotting to identify interactions between Raf and 19 putative interaction partners. A panel of 19 possible Raf interaction partners (kinases, GTPases, scaffolding proteins etc) was constructed based upon known signaling pathways. We did not consider the most likely binding partner, the small GTPase RAS, as previous studies have ruled it out in MAPK activation in HL-60 cells (25, 33). Total Raf was used as a bait protein for the immunoprecipitation studies. Interrogation of the Raf interactome thus suggested Vav1 was involved with ATRA-induced initiation of MAPK activity (Fig. 8).

Western blot analysis using total Raf and Raf-pS621 specific antibodies confirmed the presence of the bait protein, total and phosphorylated forms, in the immunoprecipitate (Fig. 8A). Of the 19 proteins sampled, Vav1, Src, CK2, Akt, and 14-3-3 co-precipitated with Raf, suggesting their co-existence in a complex was possible. However, only the associations between Raf and Vav1, and Raf and Src were ATRA-inducible (Fig. 8). The interaction between Vav1 and Raf was one of the most prominent interactions in the panel, and it was crippled by inhibiting Raf. Furthermore, the Vav1 and Src associations were correlated with Raf-pS621 abundance in the precipitate. Other proteins e.g., CK2, Akt and 14-3-3, generally bound Raf regardless of phosphorylation status or ATRA treatment. The remaining 14 proteins were expressed in whole cell lysate (Fig. 8B), but were not detectable in the immuno-precipitate with Raf IP; consistent with the potential importance of the Raf-Vav interaction for signaling, it paralleled Raf phosphorylation at S621, a putative telltale of the activated kinase. Furthermore, treatment with the Raf kinase inhibitor GW5074 following ATRA exposure reduced the association of both Vav1 with Raf and Src with Raf (Fig. 8), although the signal intensity for Src was notably weak. However, GW5074 did not influence the association of CK2 or 14-3-3 with Raf, further demonstrating their independence from Raf phosphorylation. Interestingly, the Raf-Akt interaction

235 qualitatively increased following treatment with GW5074; however, it remained unaffected  
236 by treatment with ATRA. Src family kinases are known to be important in myeloid differ-  
237 entiation (34) and their role in HL-60 differentiation has been investigated elsewhere (15).  
238 Given the existing work and variable reproducibility in the context of the Raf immuno-  
239 precipitate, we did not investigate the role of Src further in this study. Taken together,  
240 the immunoprecipitation and GW5074 results implicated Vav1 association to be corre-  
241 lated with Raf activation following ATRA-treatment. Previous studies demonstrated that  
242 a Vav1-Slp76-Cbl-CD38 complex plays an important role in ATRA-induced MAPK activa-  
243 tion and differentiation of HL-60 cells (17). Here we did not observe direct interaction of  
244 Raf with Cbl or Slp76; however, this interaction could be involved upstream. Next,  
245 we considered the effect of the Raf kinase inhibitor GW5074 on functional markers of  
246 ATRA-induced growth arrest and differentiation.

247 Inhibition of Raf kinase activity modulated MAPK activation and differentiation mark-  
248 ers following ATRA exposure (Fig. 8D-F). ATRA treatment alone statistically significantly  
249 increased the G1/G0 percentage over the untreated control, while GW5074 alone had a  
250 negligible effect on the cell cycle distribution (Fig. 8D). Surprisingly, the combination of  
251 GW5074 and ATRA statistically significantly increased the G1/G0 population ( $82 \pm 1\%$ )  
252 compared with ATRA alone ( $61 \pm 0.5\%$ ). Increased G1/G0 arrest following the combined  
253 treatment with GW5074 and ATRA was unexpected, as the combination of ATRA and the  
254 MEK inhibitor (PD98059) has been shown previously to decrease ATRA-induced growth  
255 arrest (12). However, growth arrest is not the sole indication of functional differentiation.  
256 Expression of the cell surface marker CD11b has also been shown to coincide with HL-60  
257 cells myeloid differentiation (35). We measured CD11b expression, for the various treat-  
258 ment groups, using immuno-fluorescence flow cytometry 48 hr post-treatment. As with  
259 G1/G0 arrest, ATRA alone increased CD11b expression over the untreated control, while  
260 GW5074 further enhanced ATRA-induced CD11b expression (Fig. 8E). GW5074 alone

had no statistically significant effect on CD11b expression, compared with the untreated control. Lastly, the inducible reactive oxygen species (ROS) response was used as a functional marker of differentiated neutrophils (20). We measured the ROS response induced by the phorbol ester 12-O-tetradecanoylphorbol-13-acetate (TPA) using flow cytometry. Untreated cells showed no discernible TPA response, with only  $7.0 \pm 3.0\%$  ROS induction (Fig. 8F). Cells treated with ATRA had a significantly increased TPA response,  $53 \pm 7\%$  ROS induction 48 hr post-treatment. Treatment with both ATRA and GW5074 statistically significantly reduced ROS induction ( $22 \pm 0.6\%$ ) compared to ATRA alone. Interestingly, Western blot analysis did not detect a GW5074 effect on ATRA-induced expression of p47Phox, a required upstream component of the ROS response (Fig. 8F, bottom). Thus, the inhibitory effect of GW5074 on inducible ROS might occur downstream of p47Phox expression. However, the ROS producing complex is MAPK dependent, therefore it is also possible that GW5074 inhibited ROS production by interfering with MAPK activation (in which case the p47Phox marker might not accurately reflect phenotypic conversion and differentiation).

276 **Discussion**

277 In this study, we presented an effective model of ATRA-inducible differentiation of HL-60  
278 cells. The model consisted of three modules: a signal initiation module that sensed and  
279 transformed the ATRA signal into activated cRaf-pS621 and the ATRA-RAR/RXR (Trig-  
280 ger) signals; a signal integration module that controlled the expression of upstream tran-  
281 scription factors given cRaf-pS621 and activated Trigger signals; and a phenotype mod-  
282 ule which encoded the expression of functional differentiation markers from the ATRA-  
283 inducible transcription factors. The model described the transcription and translation of  
284 genes in each module, and signaling events in each module in a growing population of  
285 HL-60 cells. Model parameters were taken from literature, however, unknown coefficients  
286 that appear in the promoter logic models were estimated from protein measurements  
287 in HL-60 cells following ATRA exposure. Despite its simplicity, the effective model cap-  
288 tured key features of the ATRA induced differentiation such as sustained MAPK activation,  
289 and bistability with respect to ATRA exposure. The model also described the expression  
290 of upstream transcription factors which regulated the expression of differentiation mark-  
291 ers. Lastly, analysis of the response of the model to perturbations identified Gfi-1 and  
292 PPAR $\gamma$  as master regulators of ATRA-induced differentiation. We also found evidence  
293 of a prominent regulatory role for a signaling molecule ATRA-inducible component of the  
294 signalsome, Vav1. Vav1 is a guanine nucleotide exchange factor for Rho family GTPases  
295 that activate pathways leading to actin cytoskeletal rearrangements and transcriptional al-  
296 terations (36). The Vav1/Raf association correlated with Raf activity, was ATRA-inducible  
297 and decreased after treatment with the Raf inhibitor GW5074.

298 Naturally occurring cell fate decisions often incorporate reinforcing feedback and bista-  
299 bility (37, 38). One of the most well studied cell fate circuits is the Mos mitogen-activated  
300 protein kinase cascade in *Xenopus* oocytes. This cascade is activated when oocytes are  
301 induced by the steroid hormone progesterone (39). The MEK-dependent activation of p42

302 MAPK stimulates the accumulation of the Mos oncoprotein, which in turn activates MEK,  
303 thereby closing the feedback loop. This is similar to the signal initiation module presented  
304 here; ATRA drives signalsome formation, which activates MAPK, which in turn leads to  
305 more signalsome activation. Thus, while HL-60 and *Xenopus* oocytes are vastly different  
306 biological models, their cell fate programs share a similar architectural feature. Reinforc-  
307 ing feedback and bistability has also been implicated in hematopoietic cell fate determi-  
308 nation. Laslo et al showed in nonmalignant myelomonocytic cells that the counter antag-  
309 onistic repressors, Gfi-1 and Egr-1/2 (whose expression is tuned by PU.1 and C/EBP $\alpha$ ),  
310 encode a bistable switch that results in a macrophage, neutrophil or a mixed lineage pop-  
311 ulation depending upon PU.1 and C/EBP $\alpha$  expression (38). The current model contained  
312 the Gfi-1 and Egr-1/2 agonistic switch; however, its significance was unclear for HL-60  
313 cells. The expression of Gfi-1, Egr-1/2, C/EBP $\alpha$  and PU.1 was not consistent with the  
314 canonical lineage pattern expected from literature. For example, Egr-1/2 expression (as-  
315 sociated with a macrophage lineage) increased, while Gfi-1 expression (associated with  
316 a neutrophil lineage) was unchanged following ATRA exposure. Thus, HL-60 cells, which  
317 are a less mature cancer cell line, exhibited a non-canonical expression pattern. Other  
318 unrelated cell fate decisions such as programmed cell death have also been suggested to  
319 be bistable (40). Still more biochemical networks important to human health, for example  
320 the human coagulation or complement cascades, also feature strong positive feedback el-  
321 ements (41). Thus, while reinforcing feedback is often undesirable in human engineered  
322 systems, it is at the core of a diverse variety of cell fate programs and other networks  
323 important to human health.

324 Analysis of the signal integration and phenotype modules suggested Gfi-1 and PPAR $\gamma$   
325 proteins were important regulators of ATRA-induced signal integration and phenotypic  
326 change. Model analysis showed that PU.1, Egr-1 and C/EBP $\alpha$  expression increased in  
327 Gfi-1 $^{-/-}$  mutants, where PU.1 expression was upregulated by greater than 8-fold. PU.1, a

member of the *ets* transcription factor family, is a well known regulator of granulocyte and monocyte development (42). The relative level of PU.1 and C/EBP $\alpha$  is thought to control macrophage versus neutrophil cell fate decisions in granulocytic macrophage progenitor cells (43). Simulations suggested that combined Gfi-1 + PPAR $\gamma$  deletion crippled the ability of HL-60 cells to undergo neutrophilic differentiation following ATRA exposure. p21 expression decreased significantly, suggesting Gfi-1 $^{-/-}$  + PPAR $\gamma$  $^{-/-}$  mutants were less likely to G0-arrest following ATRA exposure. The expression of other neutrophilic markers, such as CD38, also decreased in Gfi-1 $^{-/-}$  + PPAR $\gamma$  $^{-/-}$  cells. On the other hand, the expression of reactive oxygen metabolic markers, or other important transcription factors such as Oct4 did not change. For example, model analysis suggested that the C/EBP $\alpha$  dependent interaction of PU.1 with the *NCF1* gene, which encodes the p47Phox protein, was the most sensitive PU.1 connection; deletion of this connection removed the ability of the system to express p47Phox. p47Phox, also known as neutrophil cytosol factor 1, is one of four cytosolic subunits of the multi-protein NADPH oxidase complex found in neutrophils (44). This enzyme is responsible for reactive oxygen species (ROS) production, a key component of the anti-microbial function of neutrophils. While p47Phox expression required C/EBP $\alpha$  and PU.1, neither Gfi-1 nor PPAR $\gamma$  deletion increased expression. This suggested that p47Phox expression was saturated with respect to C/EBP $\alpha$  and PU.1, and simultaneously not sensitive to PPAR $\gamma$  abundance. Taken together, Gfi-1 $^{-/-}$  + PPAR $\gamma$  $^{-/-}$  cells were predicted to exhibit some aspects of the ATRA response, but not other critical features such as cell cycle arrest. Hock et al showed that Gfi-1 $^{-/-}$  mice lacked normal neutrophils, and were highly sensitive to bacterial infection (45). Thus, the model analysis was consistent with this study. However, other predictions concerning the behavior of the Gfi-1 $^{-/-}$  + PPAR $\gamma$  $^{-/-}$  mutants remain to be tested.

Immunoprecipitation studies identified a limited number of ATRA-dependent and - independent Raf interaction partners. While we were unable to detect the association

354 of Raf with common kinases and GTPases such as PKC, PKA, p38, Rac and Rho, we  
355 did establish potential interactions between Raf and key partners such as Vav1, Src, Akt,  
356 CK2 and 14-3-3. All of these partners are known to be associated with Raf activation  
357 or function. Src is known to bind Raf through an SH2 domain, and this association has  
358 been shown to be dependent of the serine phosphorylation of Raf (46). Thus, an ATRA in-  
359 ductible Src/Raf association may be a result of ATRA-induced Raf phosphorylation at S259  
360 or S621. We also identified an interaction between Raf and the Ser/Thr kinases Akt and  
361 CK2. Akt can phosphorylate Raf at S259, as demonstrated by studies in a human breast  
362 cancer line (47). CK2 can also phosphorylate Raf, although the literature has traditionally  
363 focused on S338 and not S621 or S259(48). However, neither of these kinase interactions  
364 were ATRA-inducible, suggesting their association with Raf alone was not associated with  
365 ATRA-induced Raf phosphorylation. The adapter protein 14-3-3 was also constitutively  
366 associated with Raf. The interaction between Raf and 14-3-3 has been associated with  
367 both S621 and S259 phosphorylation and activity (49). Additionally, the association of  
368 Raf with 14-3-3 not only stabilized S621 phosphorylation, but also reversed the S621  
369 phosphorylation from inhibitory to activating (50). Finally, we found that Vav1/Raf associ-  
370 ation correlated with Raf activity, was ATRA-inducible and decreased after treatment with  
371 GW5074. The presence of Vav1 in Raf/Grb2 complexes has been shown to correlate with  
372 increased Raf activity in mast cells (51). Furthermore, studies on Vav1 knockout mice  
373 demonstrated that the loss of Vav1 resulted in deficiencies of ERK signaling for both T-  
374 cells as well as neutrophils (52, 53). Interestingly, while an integrin ligand-induced ROS  
375 response was blocked in Vav1 knockout neutrophils, TPA was able to bypass the Vav1  
376 requirement and stimulate both ERK phosphorylation and ROS induction (53). In this  
377 study, the TPA-induced ROS response was dependent upon Raf kinase activity, and was  
378 mitigated by the addition of GW5074. It is possible that Vav1 is downstream of various  
379 integrin receptors but upstream of Raf in terms of inducible ROS responses. Vav1 has

380 also been shown to associate with a Cbl-Slp76-CD38 complex in an ATRA-dependent  
381 manner; furthermore, transfection of HL-60 cells with Cbl mutants that fail to bind CD38,  
382 yet still bind Slp76 and Vav1, prevents ATRA-induced MAPK activation (17). The literature  
383 suggest a variety of possible receptor-signaling pathways, which involve Vav1, for MAPK  
384 activation; moreover, given the ATRA-inducible association Vav1 may play a direct role in  
385 Raf activation.

386 We hypothesized that Vav1 is a member of an ATRA-inducible complex which propels  
387 sustained MAPK activation, arrest and differentiation. Initially, ATRA-induced Vav1 ex-  
388 pression drives increased association between Vav1 and Raf. This increased interaction  
389 facilitates phosphorylation and activation of Raf by pre-bound Akt and/or CK2 at S621  
390 or perhaps S259. Constitutively bound 14-3-3 may also stabilize the S621 phosphory-  
391 lation, modulate the activity and/or up-regulate autophosphorylation. Activated Raf can  
392 then drive ERK activation, which in turn closes the positive feedback loop by activating  
393 Raf transcription factors e.g., Sp1 and/or STAT1 (54–57). We tested this working hypoth-  
394 esis using mathematical modeling. The model recapitulated both ATRA time-course data  
395 as well as the GW5074 inhibitor effects. This suggested the proposed Raf-Vav1 archi-  
396 tecture was at least consistent with the experimental studies. Further, analysis of the  
397 Raf-Vav1 model identified bistability in phosphorylated ERK levels. Thus, two possible  
398 MAPK activation branches were possible for experimentally testable ATRA values. The  
399 analysis also suggested the ATRA-induced Raf-Vav1 architecture could be locked into  
400 a sustained signaling mode (high phosphorylated ERK) even in the absence of a ATRA  
401 signal. This locked-in property could give rise to an ATRA-induction memory. We val-  
402 idated the treatment memory property predicted by the Raf-Vav1 circuit experimentally  
403 using ATRA-washout experiments. ERK phosphorylation levels remained high for more  
404 than 96 hr after ATRA was removed. Previous studies demonstrated that HL-60 cells  
405 possessed an inheritable memory of ATRA stimulus (58). Although the active state was

406 self-sustaining, the inactive state demonstrated considerable robustness to perturbation.  
407 For example, we found that 50x overexpression of Raf was required to reliably lock MAPK  
408 into the activated state, while small perturbations had almost no effect on phosphorylated  
409 ERK levels over the entire ensemble. CD38 expression correlated with the phospho-  
410 rylated ERK, suggesting its involvement in the signaling complex. Our computational  
411 and experimental results showed that positive feedback, through ERK-dependent Raf ex-  
412 pression, could sustain MAPK signaling through many division cycles. Such molecular  
413 mechanisms could underly aspects of cellular memory associated to consecutive ATRA  
414 treatments.

415 **Materials and Methods**

416 *Effective gene expression model equations.* The ATRA differentiation model was en-  
417 coded as a system of differential algebraic equations (DAEs) which described signaling  
418 and gene expression processes. We modeled transcription and translation as Ordinary  
419 Differential Equations (ODEs), while signaling processes were assumed to quickly equili-  
420 brate and were treated as a pseudo steady state system of algebraic equations. We de-  
421 composed the ATRA-induced differentiation program into three modules; a signal initiation  
422 module that sensed and transformed the ATRA signal into activated cRaf-pS621 and the  
423 ATRA-RAR/RXR (activated Trigger) signals; a signal integration module that controlled the  
424 expression of upstream transcription factors given cRaf-pS621 and activated Trigger sig-  
425 nals; and a phenotype module which encoded the expression of functional differentiation  
426 markers from the ATRA-inducible transcription factors. The output of the signal initiation  
427 module was the input to the gene expression model. For each gene  $j = 1, 2, \dots, \mathcal{G}$ , we  
428 modeled both the mRNA ( $m_j$ ), protein ( $p_j$ ) and signaling species abundance:

$$\frac{dm_j}{dt} = r_{T,j} - (\mu + \theta_{m,j}) m_j + \lambda_j \quad (1)$$

$$\frac{dp_j}{dt} = r_{X,j} - (\mu + \theta_{p,j}) p_j \quad (2)$$

$$\mathbf{g}(p_1, \dots, p_{\mathcal{G}}, \kappa) = \mathbf{0} \quad (3)$$

429 where signaling species abundance was governed by the non-linear algebraic equations  
430  $\mathbf{g}(p_1, \dots, p_{\mathcal{G}}, \kappa) = \mathbf{0}$ . The model parameter vector is denoted by  $\kappa$ . The terms  $r_{T,j}$  and  
431  $r_{X,j}$  denote the specific rates of transcription, and translation while the terms  $\theta_{m,j}$  and  $\theta_{p,j}$   
432 denote first-order degradation constants for mRNA and protein, respectively. The specific  
433 transcription rate  $r_{T,j}$  was modeled as the product of a kinetic term  $\bar{r}_{T,j}$  and a control  
434 term  $u_j$  which described how the abundance of transcription factors, or other regulators

435 influenced the expression of gene  $j$ . The kinetic transcription term  $\bar{r}_{T,j}$  was modeled as:

$$\bar{r}_{T,j} = V_T^{\max} \left( \frac{L_{T,o}}{L_{T,j}} \right) \left( \frac{G_j}{K_T + G_j} \right) \quad (4)$$

436 where the maximum gene expression rate  $V_T^{\max}$  was defined as the product of a char-  
 437 acteristic transcription rate constant ( $k_T$ ) and the abundance of RNA polymerase ( $R_1$ ),  
 438  $V_T^{\max} = k_T (R_1)$ . The  $(L_{T,o}/L_{T,j})$  term denotes the ratio of transcription read lengths;  $L_{T,o}$   
 439 represents a characteristic gene length, while  $L_{T,j}$  denotes the length of gene  $j$ . Thus, the  
 440 ratio  $(L_{T,o}/L_{T,j})$  is a gene specific correction to the characteristic transcription rate  $V_T^{\max}$ .  
 441 Lastly, the  $\lambda_j$  term denotes the constitutive rate of expression of gene  $j$ .

442 The gene expression control term  $0 \leq u_j \leq 1$  depended upon the combination of fac-  
 443 tors which influenced the expression of gene  $j$ . If the expression of gene  $j$  was influenced  
 444 by  $1, \dots, m$  factors, we modeled this relationship as  $u_j = \mathcal{I}_j(f_{1j}(\cdot), \dots, f_{mj}(\cdot))$  where  
 445  $0 \leq f_{ij}(\cdot) \leq 1$  denotes a regulatory transfer function quantifying the influence of factor  $i$   
 446 on the expression of gene  $j$ , and  $\mathcal{I}_j(\cdot)$  denotes an integration rule which combines the  
 447 individual regulatory inputs for gene  $j$  into a single control term. In this study, the integra-  
 448 tion rule governing gene expression was the weighted fraction of promoter configurations  
 449 that resulted in gene expression (59):

$$u_j = \frac{W_{R_{1,j}} + \sum_n W_{nj} f_{nj}}{1 + W_{R_{1,j}} + \sum_d W_{dj} f_{dj}} \quad (5)$$

450 The numerator, the weighted sum (with weights  $W_{nj}$ ) of promoter configurations leading to  
 451 gene expression, was normalized by all possible promoter configurations. The likelihood  
 452 of each configuration was quantified by the transfer function  $f_{nj}$  (which we modeled using  
 453 Hill like functions), while the lead term in the numerator  $W_{R_{1,j}}$  denotes the weight of con-  
 454 stitutive expression for gene  $j$ . Given this formulation, the rate of constitutive expression

455 was then given by:

$$\lambda_j = \bar{r}_{T,j} \left( \frac{W_{R_1,j}}{1 + W_{R_1,j}} \right) \quad (6)$$

456 If a gene expression process had no modifying factors,  $u_j = 1$ . Lastly, the specific trans-

457 lation rate was modeled as:

$$r_{X,j} = V_X^{max} \left( \frac{L_{X,o}}{L_{X,j}} \right) \left( \frac{m_j}{K_X + m_j} \right) \quad (7)$$

458 where  $V_X^{max}$  denotes a characteristic maximum translation rate estimated from literature,

459 and  $K_X$  denotes a translation saturation constant. The characteristic maximum translation

460 rate was defined as the product of a characteristic translation rate constant ( $k_X$ ) and

461 the Ribosome abundance ( $R_2$ ),  $V_X^{max} = k_X (R_2)$ . As was the case for transcription, we

462 corrected the characteristic translation rate by the ratio of the length of a characteristic

463 transcription normalized by the length of transcript  $j$ .

464 *Signaling model equations.* The signal initiation, and integration modules required the

465 abundance of cRaf-pS621 and ATRA-RAR/RXR (activated Trigger) as inputs. However,

466 our base model described only the abundance of inactive proteins e.g., cRaf or RXR/RAR

467 but not the activated forms. To address this issue, we estimated pseudo steady state

468 approximations for the abundance of cRaf-pS621 and activated Trigger. The abundance

469 of activated trigger ( $x_{a,1}$ ) was estimated directly from the RXR/RAR abundance ( $x_{u,1}$ ):

$$x_{a,1} \sim x_{u,1} \left( \frac{\alpha \cdot \text{ATRA}}{1 + \alpha \cdot \text{ATRA}} \right) \quad (8)$$

470 where  $\alpha$  denotes a gain parameter;  $\alpha = 0.0$  if ATRA is less than a threshold, and  $\alpha = 0.1$

471 if ATRA is greater than the differentiation threshold. The abundance of cRaf-pS621 was

472 estimated by making the pseudo steady state approximation on the cRaf-pS621 balance.

473 The abundance of an activated signaling species  $i$  was given by:

$$\frac{dx_i}{dt} = r_{+,i}(\mathbf{x}, \mathbf{k}) - (\mu + k_{d,i}) x_i \quad i = 1, \dots, \mathcal{M} \quad (9)$$

474 The quantity  $x_i$  denotes concentration of signaling species  $i$ , while  $\mathcal{R}$  and  $\mathcal{M}$  denote  
 475 the number of signaling reactions and signaling species in the model, respectively. The  
 476 term  $r_{+,i}(\mathbf{x}, \mathbf{k})$  denotes the rate of generation of activated species  $i$ , while  $\mu$  denotes  
 477 the specific growth rate, and  $k_{d,i}$  denotes the rate constant controlling the non-specific  
 478 degradation of  $x_i$ . We neglected deactivation reactions e.g., phosphatase activities. We  
 479 assumed that signaling processes were fast compared to gene expression; this allowed  
 480 us to approximate the signaling balance as:

$$x_i^* \simeq \frac{r_{+,i}(\mathbf{x}, \mathbf{k})}{(\mu + k_{d,i})} \quad i = 1, \dots, \mathcal{M} \quad (10)$$

481 The generation rate was written as the product of a kinetic term ( $\bar{r}_{+,i}$ ) and a control term  
 482 ( $v_i$ ). The control terms  $0 \leq v_j \leq 1$  depended upon the combination of factors which in-  
 483 fluenced rate process  $j$ . If rate  $j$  was influenced by  $1, \dots, m$  factors, we modeled this  
 484 relationship as  $v_j = \mathcal{I}_j(f_{1j}(\cdot), \dots, f_{mj}(\cdot))$  where  $0 \leq f_{ij}(\cdot) \leq 1$  denotes a regulatory  
 485 transfer function quantifying the influence of factor  $i$  on rate  $j$ . The function  $\mathcal{I}_j(\cdot)$  is an  
 486 integration rule which maps the output of regulatory transfer functions into a control vari-  
 487 able. In this study, we used  $\mathcal{I}_j \in \{\min, \max\}$  and hill transfer functions (60). If a process  
 488 had no modifying factors,  $v_j = 1$ . The kinetic rate of cRaf-pS621 generation  $\bar{r}_{+,cRaf}$  was  
 489 modeled as:

$$\bar{r}_{+,cRaf} = k_{+,cRaf} x_s \left( \frac{x_{cRaf}}{K_{+,cRaf} + x_{cRaf}} \right) \quad (11)$$

490 where  $x_s$  denotes the signalsome abundance, and  $K_{+,cRaf}$  denotes a saturation constant  
 491 governing cRaf-pS621 formation. In this study, signalsome abundance was approxi-

492 mated by the abundance of the BLR1 protein; BLR1 expression is directly related to Raf  
 493 nuclear translocation which in turn is related to activated signalsome. Thus, BLR1 is an  
 494 indirect measure of the signalsome. The formation of cRaf-pS621 was regulated by only  
 495 a single factor, the abundance of MAPK inhibitor, thus  $v_{+,cRaf}$  took the form:

$$v_{+,cRaf} = \left(1 - \frac{I}{K_D + I}\right) \quad (12)$$

496 where  $I$  denotes the abundance of the MAPK inhibitor, and  $K_D$  denotes the inhibitor  
 497 affinity.

498 *Estimation of gene expression model parameters.* We estimated parameters appearing  
 499 in the mRNA and protein balances, the abundance of polymerases and ribosomes, tran-  
 500 scription and translation rates, the half-life of a typical mRNA and protein, and typical  
 501 values for the copies per cell of RNA polymerase and ribosomes from literature (Table 2).  
 502 The saturation constants  $K_X$  and  $K_T$  were adjusted so that gene expression and trans-  
 503 lation resulted in gene products on a biologically realistic concentration scale. Lastly, we  
 504 calculated the concentration for gene  $G_j$  by assuming, on average, that a cell had two  
 505 copies of each gene at any given time. Thus, the bulk of our gene expression model pa-  
 506 rameters were based directly upon literature values, and were not adjusted during model  
 507 identification. However, the remaining parameters, e.g., the  $W_{ij}$  appearing in the gene  
 508 expression control laws, or parameters appearing in the transfer functions  $f_{dij}$ , were esti-  
 509 mated from the protein expression and signaling data sets discussed here.

510 Signaling and gene expression model parameters were estimated by minimizing the  
 511 squared difference between simulations and experimental protein data set  $j$ . We mea-  
 512 sured the squared difference in the scale, fold change and shape for protein  $j$ :

$$E_j(\mathbf{k}) = \left( \mathcal{M}_j(t_-) - \hat{y}_j(t_-, \mathbf{k}) \right)^2 + \sum_{i=1}^{\mathcal{T}_j} \left( \hat{\mathcal{M}}_{ij} - \hat{y}_{ij}(\mathbf{k}) \right)^2 + \sum_{i=1}^{\mathcal{T}_j} \left( \mathcal{M}'_{ij} - y'_{ij}(\mathbf{k}) \right)^2 \quad (13)$$

513 The first term in Eq. (13) quantified the initial *scale* error, directly before the addition  
 514 of ATRA. In this case,  $\mathcal{M}_j(t_-)$  (the approximate concentration of protein  $j$  before the  
 515 addition of ATRA) was estimated from literature. This term was required because the  
 516 protein measurements were reported as the fold-change; thus, the data was normalized  
 517 by a control value measured before the addition of ATRA. However, the model operated on  
 518 a physical scale. The first term allowed the model to capture physically realistic changes  
 519 following ATRA addition. The second term quantified the difference in the *fold-change* of  
 520 protein  $j$  as a function of time. The terms  $\hat{\mathcal{M}}_{ij}$  and  $\hat{y}_{ij}$  denote the scaled experimental  
 521 observations and simulation outputs (fold-change; protein normalized by control value  
 522 directly before ATRA addition) at time  $i$  from protein  $j$ , where  $T_j$  denoted the number of  
 523 time points for data set  $j$ . Lastly, the third term of the objective function measured the  
 524 difference in the *shape* of the measured and simulated protein levels. The scaled value  
 525  $0 \leq \mathcal{M}'_{ij} \leq 1$  was given by:

$$\hat{\mathcal{M}}_{ij} = \left( \mathcal{M}_{ij} - \min_i \mathcal{M}_{ij} \right) / \left( \max_i \mathcal{M}_{ij} - \min_i \mathcal{M}_{ij} \right) \quad (14)$$

526 where  $\mathcal{M}'_{ij} = 0$  and  $\mathcal{M}'_{ij} = 1$  describe the lowest (highest) intensity bands. A similar  
 527 scaling was used for the simulation output. We minimized the total model residual  $\sum_j E_j$   
 528 using a heuristic direct-search optimization procedure, subject to box constraints on the  
 529 parameter values, starting from a random initial parameter guess. Each downhill step was  
 530 archived and used for ensemble calculations. The optimization procedure (a covariance  
 531 matrix adaptation evolution strategy) has been reported previously (61).

532 *Estimation of an effective cell cycle arrest model.* We formulated an effective N-order  
 533 polynomial model of the fraction of cells undergoing ATRA-induced cell cycle arrest at  
 534 time  $t$ ,  $\hat{\mathcal{A}}(t)$ , as:

$$\hat{\mathcal{A}}(t) \simeq a_0 + \sum_{i=1}^{N-1} a_i \phi_i(\mathbf{p}(t), t) \quad (15)$$

535 where  $a_i$  were unknown parameters, and  $\phi_i(\mathbf{p}(t), t)$  denotes a basis function. The basis  
536 functions were dependent upon the system state; in this study, we used N = 4 and basis  
537 functions of the form:

$$\phi_i(\mathbf{p}(t), t) = \left( \frac{t}{T} + \frac{p21}{E2F} \Big|_t \right)^{(i-1)} \quad (16)$$

538 The parameters  $a_0, \dots, a_3$  were estimated directly from cell-cycle measurements (biolog-  
539 ical replicates) using least-squares. The form of the basis function assumed p21 was  
540 directly proportional, and E2F inversely proportional, to G0-arrest. However, this was one  
541 of many possible forms for the basis functions.

542 *Availability of the model code and parameters.* The signaling and gene expression model  
543 equations, and the parameter estimation procedure, were implemented in the Julia pro-  
544 gramming language. The model equations were solved using the ODE23s routine of the  
545 ODE package (62). The model code and parameter ensemble is available under an MIT  
546 software license and can be downloaded from <http://www.varnerlab.org>.

547 *Cell culture and treatment* Human myeloblastic leukemia cells (HL-60 cells) were grown  
548 in a humidified atmosphere of 5% CO<sub>2</sub> at 37°C and maintained in RPMI 1640 from Gibco  
549 (Carlsbad, CA) supplemented with 5% heat inactivated fetal bovine serum from Hyclone  
550 (Logan, UT) and 1× antibiotic/antimicotic (Gibco, Carlsbad, CA). Cells were cultured in  
551 constant exponential growth (63). Experimental cultures were initiated at  $0.1 \times 10^6$  cells/mL  
552 24 hr prior to ATRA treatment; if indicated, cells were also treated with GW5074 (2 μM) 18  
553 hr before ATRA treatment. For the cell culture washout experiments, cells were treated  
554 with ATRA for 24 hr, washed 3x with prewarmed serum supplemented culture medium  
555 to remove ATRA, and reseeded in ATRA-free media as described. Western blot analysis  
556 was performed at incremental time points after removal of ATRA.

557 *Chemicals* All-Trans Retinoic Acid (ATRA) from Sigma-Aldrich (St. Louis, MO) was dis-  
558 solved in 100% ethanol with a stock concentration of 5mM, and used at a final concen-

559 tration of 1 $\mu$ M (unless otherwise noted). The cRaf inhibitor GW5074 from Sigma-Aldrich  
560 (St. Louis, MO) was dissolved in DMSO with a stock concentration of 10mM, and used  
561 at a final concentration of 2 $\mu$ M. HL-60 cells were treated with 2 $\mu$ M GW5074 with or with-  
562 out ATRA (1 $\mu$ M) at 0 hr. This GW5074 dosage had a negligible effect on the cell cycle  
563 distribution, compared to ATRA treatment alone.

564 *Immunoprecipitation and western blotting* For immunoprecipitation experiments, cells  
565 were lysed as previously described. 300 $\mu$ g protein (in 300  $\mu$ L total volume) per sam-  
566 ple was pre-cleared with Protein A/G beads. The beads were pelleted and supernatant  
567 was incubated with Raf antibody (3 $\mu$ L/sample) and beads overnight. All incubations in-  
568 cluded protease and phosphatase inhibitors in M-PER used for lysis with constant rota-  
569 tion at 4°C. Bead/antibody/protein slurries were then washed and subjected to standard  
570 SDS-PAGE analysis as previously described (17). All antibodies were purchased from  
571 Cell Signaling (Boston, MA) with the exception of  $\alpha$ -p621 Raf which was purchased from  
572 Biosource/Invitrogen (Carlsbad, CA), and  $\alpha$ -CK2 from BD Biosciences (San Jose, CA).

573 *Morphology assessment* Untreated and ATRA-treated HL-60 cells were collected after  
574 72 hr and cytocentrifuged for 3 min at 700 rpm onto glass slides. Slides were air-dried  
575 and stained with Wright's stain. Slide images were captured at 40X (Leica DM LB 100T  
576 microscope, Leica Microsystems).

577 **Competing interests**

578 The authors declare that they have no competing interests.

579 **Author's contributions**

580 J.V and A.Y directed the study. R.T, H.J, R.B and J.C conducted the cell culture measure-  
581 ments. J.V, R.B, W.D, K.R and A.S developed the reduced order HL-60 models and the  
582 parameter ensemble. W.D and J.V analyzed the model ensemble, and generated figures  
583 for the manuscript. The manuscript was prepared and edited for publication by W.D, R.B,  
584 A.Y and J.V.

585 **Acknowledgements**

586 We gratefully acknowledge the suggestions from the anonymous reviewers to improve  
587 this manuscript.

588 **Funding**

589 We acknowledge the financial support to J.V. by the National Science Foundation CA-  
590 REER (CBET-0846876) for the support of R.T. and H.J. In addition, we acknowledge  
591 support to A.Y. from the National Institutes of Health (CA 30555, CA152870) and a grant  
592 from New York State Stem Cell Science. Lastly, we acknowledge the financial support to  
593 J.V. and A.Y. from the National Cancer Institute (#U54 CA143876). The content is solely  
594 the responsibility of the authors and does not necessarily represent the official views of  
595 the National Cancer Institute or the National Institutes of Health.

596 **References**

- 597 1. Bushue N, Wan YJY (2010) Retinoid pathway and cancer therapeutics. *Adv Drug  
598 Deliv Rev* 62: 1285-98.
- 599 2. Tang XH, Gudas LJ (2011) Retinoids, retinoic acid receptors, and cancer. *Annu Rev  
600 Pathol* 6: 345-64.
- 601 3. Cheung FSG, Lovicu FJ, Reichardt JKV (2012) Current progress in using vitamin d  
602 and its analogs for cancer prevention and treatment. *Expert Rev Anticancer Ther*  
603 12: 811-37.
- 604 4. Uray IP, Dmitrovsky E, Brown PH (2016) Retinoids and rexinoids in cancer preven-  
605 tion: from laboratory to clinic. *Semin Oncol* 43: 49-64.
- 606 5. Li C, Imai M, Hasegawa S, Yamasaki M, Takahashi N (2017) Growth inhibition of  
607 refractory human gallbladder cancer cells by retinol, and its mechanism of action.  
608 *Biol Pharm Bull* 40: 495-503.
- 609 6. Nilsson B (1984) Probable in vivo induction of differentiation by retinoic acid of  
610 promyelocytes in acute promyelocytic leukaemia. *Br J Haematol* 57: 365-71.
- 611 7. Coombs CC, Tavakkoli M, Tallman MS (2015) Acute promyelocytic leukemia: where  
612 did we start, where are we now, and the future. *Blood Cancer J* 5: e304.
- 613 8. Warrell RP Jr (1993) Retinoid resistance in acute promyelocytic leukemia: new  
614 mechanisms, strategies, and implications. *Blood* 82: 1949-53.
- 615 9. Freemantle SJ, Spinella MJ, Dmitrovsky E (2003) Retinoids in cancer therapy and  
616 chemoprevention: promise meets resistance. *Oncogene* 22: 7305-15.
- 617 10. Harrison JS, Wang X, Studzinski GP (2016) The role of vdr and bim in potentiation  
618 of cytarabine-induced cell death in human aml blasts. *Oncotarget* 7: 36447-36460.
- 619 11. Breitman TR, Selonick SE, Collins SJ (1980) Induction of differentiation of the hu-  
620 man promyelocytic leukemia cell line (HL-60) by retinoic acid. *Proc Natl Acad Sci U  
621 S A* 77: 2936–2940.

- 622 12. Yen A, Roberson MS, Varvayanis S, Lee AT (1998) Retinoic acid induced  
623 mitogen-activated protein (MAP)/extracellular signal-regulated kinase (ERK) kinase-  
624 dependent MAP kinase activation needed to elicit HL-60 cell differentiation and  
625 growth arrest. *Cancer Res* 58: 3163–3172.
- 626 13. Hong HY, Varvayanis S, Yen A (2001) Retinoic acid causes MEK-dependent RAF  
627 phosphorylation through RARalpha plus RXR activation in HL-60 cells. *Differentiation*  
628 68: 55–66.
- 629 14. Mangelsdorf DJ, Ong ES, Dyck JA, Evans RM (1990) Nuclear receptor that identifies  
630 a novel retinoic acid response pathway. *Nature* 345: 224–229.
- 631 15. Congleton J, MacDonald R, Yen A (2012) Src inhibitors, PP2 and dasatinib, increase  
632 retinoic acid-induced association of Lyn and c-Raf (S259) and enhance MAPK-  
633 dependent differentiation of myeloid leukemia cells. *Leukemia* 26: 1180-8.
- 634 16. Shen M, Bunaci R, Congleton J, Jensen H, Sayam L, et al. (2011) Interferon regu-  
635 latory factor-1 binds c-Cbl, enhances mitogen activated protein kinase signaling and  
636 promotes retinoic acid-induced differentiation of HL-60 human myelo-monoblastic  
637 leukemia cells. *Leuk Lymphoma* 52: 2372-9.
- 638 17. Shen M, Yen A (2009) c-cbl tyrosine kinase-binding domain mutant g306e abolishes  
639 the interaction of c-cbl with cd38 and fails to promote retinoic acid-induced cell dif-  
640 ferentiation and g0 arrest. *J Biol Chem* 284: 25664-77.
- 641 18. Yen A, Varvayanis S, Smith J, Lamkin T (2006) Retinoic acid induces expression of  
642 SLP-76: expression with c-FMS enhances ERK activation and retinoic acid-induced  
643 differentiation/G0 arrest of HL-60 cells. *Eur J Cell Biol* 85: 117–132.
- 644 19. Marchisio M, Bertagnolo V, Colamussi ML, Capitani S, Neri LM (1998) Phos-  
645 phatidylinositol 3-kinase in HL-60 nuclei is bound to the nuclear matrix and increases  
646 during granulocytic differentiation. *Biochem Biophys Res Commun* 253: 346-51.
- 647 20. Congleton J, Jiang H, Malavasi F, Lin H, Yen A (2011) ATRA-induced HL-60 myeloid

- leukemia cell differentiation depends on the CD38 cytosolic tail needed for membrane localization, but CD38 enzymatic activity is unnecessary. *Exp Cell Res* 317: 910–919.
21. Wang J, Yen A (2004) A novel retinoic acid-responsive element regulates retinoic acid induced BLR1 expression. *Mol Cell Biol* 24: 2423 - 2443.
  22. Yen A (1990) HL-60 cells as a model of growth and differentiation: the significance of variant cells. *Hematology Review* 4: 5-46.
  23. Yang T, Xiong Q, Enslen H, Davis R, Chow CW (2002) Phosphorylation of NFATc4 by p38 mitogen-activated protein kinases. *Mol Cell Biol* 22: 3892–3904.
  24. Li X, Guo C, Li Y, Li L, Wang Y, et al. (2017) Ketamine administered pregnant rats impair learning and memory in offspring via the creb pathway. *Oncotarget* .
  25. Wang J, Yen A (2008) A MAPK-positive Feedback Mechanism for BLR1 Signaling Propels Retinoic Acid-triggered Differentiation and Cell Cycle Arrest. *J Biol Chem* 283: 4375–4386.
  26. Geil WM, Yen A (2014) Nuclear raf-1 kinase regulates the cxcr5 promoter by associating with nfatc3 to drive retinoic acid-induced leukemic cell differentiation. *FEBS J* 281: 1170-80.
  27. Tasseeff R, Nayak S, Song S, Yen A, Varner J (2011) Modeling and analysis of retinoic acid induced differentiation of uncommitted precursor cells. *Integr Biol* 3: 578 - 591.
  28. Jensen HA, Styskal LE, Tasseeff R, Bunaciu RP, Congleton J, et al. (2013) The src-family kinase inhibitor pp2 rescues inducible differentiation events in emergent retinoic acid-resistant myeloblastic leukemia cells. *PLoS One* 8: e58621.
  29. Jensen HA, Bunaciu RP, Ibabao CN, Myers R, Varner JD, et al. (2014) Retinoic acid therapy resistance progresses from unilineage to bilineage in hl-60 leukemic blasts. *PLoS One* 9: e98929.
  30. Jensen HA, Bunaciu RP, Varner JD, Yen A (2015) Gw5074 and pp2 kinase inhibitors

- 674 implicate nontraditional c-raf and lyn function as drivers of retinoic acid-induced mat-  
675 uration. *Cell Signal* 27: 1666-75.
- 676 31. Jensen HA, Yourish HB, Bunaciu RP, Varner JD, Yen A (2015) Induced myelomonocytic  
677 differentiation in leukemia cells is accompanied by noncanonical transcription  
678 factor expression. *FEBS Open Bio* 5: 789-800.
- 679 32. Milo R, Jorgensen P, Moran U, Weber G, Springer M (2010) Bionumbers—the  
680 database of key numbers in molecular and cell biology. *Nucleic Acids Res* 38: D750-  
681 3.
- 682 33. Katagiri K, Hattori S, Nakamura S, Yamamoto T, Yoshida T, et al. (1994) Activation  
683 of ras and formation of gap complex during tpa-induced monocytic differentiation of  
684 hl-60 cells. *Blood* 84: 1780–1789.
- 685 34. Miranda MB, Johnson DE (2007) Signal transduction pathways that contribute to  
686 myeloid differentiation. *Leukemia* 21: 1363–1377.
- 687 35. Hickstein DD, Back AL, Collins SJ (1989) Regulation of expression of the cd11b and  
688 cd18 subunits of the neutrophil adherence receptor during human myeloid differen-  
689 tiation. *J Biol Chem* 264: 21812–21817.
- 690 36. Hornstein I, Alcover A, Katzav S (2004) Vav proteins, masters of the world of cy-  
691 toskeleton organization. *Cell Signal* 16: 1-11.
- 692 37. Ferrell J (2002) Self-perpetuating states in signal transduction: positive feedback,  
693 double-negative feedback and bistability. *Curr Opin Cell Biol* 14: 140-8.
- 694 38. Laslo P, Spooner CJ, Warmflash A, Lancki DW, Lee HJ, et al. (2006) Multilineage  
695 transcriptional priming and determination of alternate hematopoietic cell fates. *Cell*  
696 126: 755-66.
- 697 39. Xiong W, Ferrell J (2003) A positive-feedback-based bistable 'memory module' that  
698 governs a cell fate decision. *Nature* 426: 460-5.
- 699 40. Bagci EZ, Vodovotz Y, Billiar TR, Ermentrout GB, Bahar I (2006) Bistability in apop-

700                      tosis: roles of bax, bcl-2, and mitochondrial permeability transition pores. *Biophys J*  
701                      90: 1546-59.

- 702 41. Luan D, Zai M, Varner JD (2007) Computationally derived points of fragility of a  
703 human cascade are consistent with current therapeutic strategies. PLoS Comput  
704 Biol 3: e142.

705 42. Friedman AD (2007) Transcriptional control of granulocyte and monocyte develop-  
706 ment. Oncogene 26: 6816-28.

707 43. Dahl R, Walsh JC, Lancki D, Laslo P, Iyer SR, et al. (2003) Regulation of macrophage  
708 and neutrophil cell fates by the PU.1:C/EBPalpha ratio and granulocyte colony-  
709 stimulating factor. Nat Immunol 4: 1029-36.

710 44. El-Benna J, Dang PMC, Gougerot-Pocidalo MA, Marie JC, Braut-Boucher F (2009)  
711 p47phox, the phagocyte nadph oxidase/nox2 organizer: structure, phosphorylation  
712 and implication in diseases. Exp Mol Med 41: 217-25.

713 45. Hock H, Hamblen MJ, Rooke HM, Traver D, Bronson RT, et al. (2003) Intrinsic re-  
714 quirement for zinc finger transcription factor gfi-1 in neutrophil differentiation. Immu-  
715 nity 18: 109-20.

716 46. Cleghon V, Morrison DK (1994) Raf-1 interacts with fyn and src in a non-  
717 phosphotyrosine-dependent manner. J Biol Chem 269: 17749–17755.

718 47. Zimmermann S, Moelling K (1999) Phosphorylation and regulation of raf by akt (pro-  
719 tein kinase b). Science 286: 1741–1744.

720 48. Ritt DA, Zhou M, Conrads TP, Veenstra TD, Copeland TD, et al. (2007) Ck2 is a  
721 component of the ksr1 scaffold complex that contributes to raf kinase activation.  
722 Curr Biol 17: 179–184.

723 49. Hekman M, Wiese S, Metz R, Albert S, Troppmair J, et al. (2004) Dynamic changes  
724 in c-raf phosphorylation and 14-3-3 protein binding in response to growth factor stim-  
725 ulation: differential roles of 14-3-3 protein binding sites. J Biol Chem 279: 14074–

- 726 14086.
- 727 50. Dhillon AS, Yip YY, Grindlay GJ, Pakay JL, Dangers M, et al. (2009) The c-terminus  
728 of raf-1 acts as a 14-3-3-dependent activation switch. *Cell Signal* 21: 1645–1651.
- 729 51. Song JS, Gomez J, Stancato LF, Rivera J (1996) Association of a p95 vav-containing  
730 signaling complex with the fcepsilonri gamma chain in the rbl-2h3 mast cell line.  
731 evidence for a constitutive in vivo association of vav with grb2, raf-1, and erk2 in an  
732 active complex. *J Biol Chem* 271: 26962–26970.
- 733 52. Costello PS, Walters AE, Mee PJ, Turner M, Reynolds LF, et al. (1999) The rho-  
734 family gtp exchange factor vav is a critical transducer of t cell receptor signals to the  
735 calcium, erk, and nf-kappab pathways. *Proc Natl Acad Sci U S A* 96: 3035–3040.
- 736 53. Graham D, Robertson C, Bautista J, Mascarenhas F, Diacovo M, et al. (2007)  
737 Neutrophil-mediated oxidative burst and host defense are controlled by a Vav-  
738 PLCgamma2 signaling axis in mice. *J Clin Invest* 117: 3445–3452.
- 739 54. Kim HS, Lim IK (2009) Phosphorylated extracellular signal-regulated protein kinases  
740 1 and 2 phosphorylate sp1 on serine 59 and regulate cellular senescence via tran-  
741 scription of p21sdi1/cip1/waf1. *J Biol Chem* 284: 15475–15486.
- 742 55. Milanini-Mongiat J, Pouyss?gur J, Pag?o G (2002) Identification of two sp1 phos-  
743 phorylation sites for p42/p44 mitogen-activated protein kinases: their implication in  
744 vascular endothelial growth factor gene transcription. *J Biol Chem* 277: 20631–  
745 20639.
- 746 56. Zhang Y, Cho YY, Petersen BL, Zhu F, Dong Z (2004) Evidence of stat1 phosphory-  
747 lation modulated by mapks, mek1 and msk1. *Carcinogenesis* 25: 1165–1175.
- 748 57. Li Z, Theus MH, Wei L (2006) Role of erk 1/2 signaling in neuronal differentiation of  
749 cultured embryonic stem cells. *Dev Growth Differ* 48: 513–523.
- 750 58. Yen A, Reece SL, Albright KL (1984) Dependence of hl-60 myeloid cell differentiation  
751 on continuous and split retinoic acid exposures: precommitment memory associated

- 752 with altered nuclear structure. *J Cell Physiol* 118: 277–286.
- 753 59. Moon TS, Lou C, Tamsir A, Stanton BC, Voigt CA (2012) Genetic programs con-  
754 structed from layered logic gates in single cells. *Nature* 491: 249-53.
- 755 60. Wayman JA, Sagar A, Varner JD (2015) Dynamic modeling of cell-free biochemical  
756 networks using effective kinetic models. *Processes* 3: 138.
- 757 61. Igel C, Hansen N, Roth S (2007) Covariance matrix adaptation for multi-objective  
758 optimization. *Evol Comput* 15: 1-28.
- 759 62. Bezanson J, Edelman A, Karpinski S, Shah VB (2014) Julia: A fresh approach to  
760 numerical computing. *CoRR* abs/1411.1607.
- 761 63. Brooks SC, Kazmer S, Levin AA, Yen A (1996) Myeloid differentiation and retinoblas-  
762 toma phosphorylation changes in HL-60 cells induced by retinoic acid receptor- and  
763 retinoid X receptor-selective retinoic acid analogs. *Blood* 87: 227–237.
- 764 64. Rishi AK, Gerald TM, Shao ZM, Li XS, Baumann RG, et al. (1996) Regulation of the  
765 human retinoic acid receptor alpha gene in the estrogen receptor negative human  
766 breast carcinoma cell lines skbr-3 and mda-mb-435. *Cancer Res* 56: 5246-52.
- 767 65. Mueller BU, Pabst T, Fos J, Petkovic V, Fey MF, et al. (2006) Atra resolves the dif-  
768 ferentiation block in t(15;17) acute myeloid leukemia by restoring pu.1 expression.  
769 *Blood* 107: 3330-8.
- 770 66. Luo XM, Ross AC (2006) Retinoic acid exerts dual regulatory actions on the ex-  
771 pression and nuclear localization of interferon regulatory factor-1. *Exp Biol Med*  
772 (Maywood) 231: 619-31.
- 773 67. Sylvester I, Schöler HR (1994) Regulation of the oct-4 gene by nuclear receptors.  
774 *Nucleic Acids Res* 22: 901-11.
- 775 68. Drach J, McQueen T, Engel H, Andreeff M, Robertson KA, et al. (1994) Retinoic  
776 acid-induced expression of cd38 antigen in myeloid cells is mediated through  
777 retinoic acid receptor-alpha. *Cancer Res* 54: 1746-52.

- 778 69. Liu M, Iavarone A, Freedman LP (1996) Transcriptional activation of the human  
779 p21(waf1/cip1) gene by retinoic acid receptor. correlation with retinoid induction of  
780 u937 cell differentiation. J Biol Chem 271: 31723-8.
- 781 70. Bunaciu RP, Yen A (2013) 6-formylindolo (3,2-b)carbazole (ficz) enhances retinoic  
782 acid (ra)-induced differentiation of hl-60 myeloblastic leukemia cells. Mol Cancer 12:  
783 39.
- 784 71. Balmer JE, Blomhoff R (2002) Gene expression regulation by retinoic acid. J Lipid  
785 Res 43: 1773-808.
- 786 72. Rosen ED, Hsu CH, Wang X, Sakai S, Freeman MW, et al. (2002) C/ebpalpha in-  
787 duces adipogenesis through ppargamma: a unified pathway. Genes Dev 16: 22-6.
- 788 73. Varley CL, Bacon EJ, Holder JC, Southgate J (2009) Foxa1 and irf-1 intermediary  
789 transcriptional regulators of ppargamma-induced urothelial cytodifferentiation. Cell  
790 Death Differ 16: 103-14.
- 791 74. Bruemmer D, Yin F, Liu J, Berger JP, Sakai T, et al. (2003) Regulation of the growth  
792 arrest and dna damage-inducible gene 45 (gadd45) by peroxisome proliferator-  
793 activated receptor gamma in vascular smooth muscle cells. Circ Res 93: e38-47.
- 794 75. Delerive P, De Bosscher K, Besnard S, Vanden Berghe W, Peters JM, et al. (1999)  
795 Peroxisome proliferator-activated receptor alpha negatively regulates the vascular  
796 inflammatory gene response by negative cross-talk with transcription factors nf-  
797 kappaB and ap-1. J Biol Chem 274: 32048-54.
- 798 76. Altinok S, Xu M, Spiegelman BM (1997) Ppargamma induces cell cycle withdrawal:  
799 inhibition of e2f/dp dna-binding activity via down-regulation of pp2a. Genes Dev 11:  
800 1987-98.
- 801 77. Fei J, Cook C, Gillespie M, Yu B, Fullen K, et al. (2011) Atherogenic  $\omega$ -6 lipids mod-  
802 ulate ppar- egr-1 crosstalk in vascular cells. PPAR Res 2011: 753917.
- 803 78. Song EK, Lee YR, Kim YR, Yeom JH, Yoo CH, et al. (2012) Naadp mediates insulin-

- 804 stimulated glucose uptake and insulin sensitization by ppar $\gamma$  in adipocytes. Cell Rep  
805 2: 1607-19.
- 806 79. Szanto A, Nagy L (2005) Retinoids potentiate peroxisome proliferator-activated re-  
807 ceptor gamma action in differentiation, gene expression, and lipid metabolic pro-  
808 cesses in developing myeloid cells. Mol Pharmacol 67: 1935-43.
- 809 80. Han S, Sidell N, Fisher PB, Roman J (2004) Up-regulation of p21 gene expres-  
810 sion by peroxisome proliferator-activated receptor gamma in human lung carcinoma  
811 cells. Clin Cancer Res 10: 1911-9.
- 812 81. Von Knethen A, Brüne B (2002) Activation of peroxisome proliferator-activated re-  
813 ceptor gamma by nitric oxide in monocytes/macrophages down-regulates p47phox  
814 and attenuates the respiratory burst. J Immunol 169: 2619-26.
- 815 82. Dispirito JR, Fang B, Wang F, Lazar MA (2013) Pruning of the adipocyte peroxisome  
816 proliferator-activated receptor  $\gamma$  cistrome by hematopoietic master regulator pu.1.  
817 Mol Cell Biol 33: 3354-64.
- 818 83. Chen H, Ray-Gallet D, Zhang P, Hetherington CJ, Gonzalez DA, et al. (1995) Pu.1  
819 (spi-1) autoregulates its expression in myeloid cells. Oncogene 11: 1549-60.
- 820 84. Steidl U, Rosenbauer F, Verhaak RGW, Gu X, Ebralidze A, et al. (2006) Essential  
821 role of jun family transcription factors in pu.1 knockdown-induced leukemic stem  
822 cells. Nat Genet 38: 1269-77.
- 823 85. Pahl HL, Scheibe RJ, Zhang DE, Chen HM, Galson DL, et al. (1993) The proto-  
824 oncogene pu.1 regulates expression of the myeloid-specific cd11b promoter. J Biol  
825 Chem 268: 5014-20.
- 826 86. Yuki H, Ueno S, Tatetsu H, Niilo H, Iino T, et al. (2013) Pu.1 is a potent tumor  
827 suppressor in classical hodgkin lymphoma cells. Blood 121: 962-70.
- 828 87. Li SL, Schlegel W, Valente AJ, Clark RA (1999) Critical flanking sequences of pu.1  
829 binding sites in myeloid-specific promoters. J Biol Chem 274: 32453-60.

- 830 88. Timchenko N, Wilson DR, Taylor LR, Abdelsayed S, Wilde M, et al. (1995) Autoreg-  
831 ulation of the human c/ebp alpha gene by stimulation of upstream stimulatory factor  
832 binding. Mol Cell Biol 15: 1192-202.
- 833 89. Lidonnici MR, Audia A, Soliera AR, Prisco M, Ferrari-Amorotti G, et al. (2010) Ex-  
834 pression of the transcriptional repressor gfi-1 is regulated by c/ebpalpha and is  
835 involved in its proliferation and colony formation-inhibitory effects in p210bcr/abl-  
836 expressing cells. Cancer Res 70: 7949-59.
- 837 90. D'Alo' F, Johansen LM, Nelson EA, Radomska HS, Evans EK, et al. (2003) The  
838 amino terminal and e2f interaction domains are critical for c/ebp alpha-mediated  
839 induction of granulopoietic development of hematopoietic cells. Blood 102: 3163-  
840 71.
- 841 91. Pan Z, Hetherington CJ, Zhang DE (1999) Ccaat/enhancer-binding protein activates  
842 the cd14 promoter and mediates transforming growth factor beta signaling in mono-  
843 cyte development. J Biol Chem 274: 23242-8.
- 844 92. Harris TE, Albrecht JH, Nakanishi M, Darlington GJ (2001) Ccaat/enhancer-binding  
845 protein-alpha cooperates with p21 to inhibit cyclin-dependent kinase-2 activity and  
846 induces growth arrest independent of dna binding. J Biol Chem 276: 29200-9.
- 847 93. Bauvois B, Durant L, Laboureau J, Barthélémy E, Rouillard D, et al. (1999) Upreg-  
848 ulation of cd38 gene expression in leukemic b cells by interferon types i and ii. J  
849 Interferon Cytokine Res 19: 1059-66.
- 850 94. Passioura T, Dolnikov A, Shen S, Symonds G (2005) N-ras-induced growth suppres-  
851 sion of myeloid cells is mediated by irf-1. Cancer Res 65: 797-804.
- 852 95. Dahl R, Iyer SR, Owens KS, Cuylear DD, Simon MC (2007) The transcriptional  
853 repressor gfi-1 antagonizes pu.1 activity through protein-protein interaction. J Biol  
854 Chem 282: 6473-83.
- 855 96. Duan Z, Horwitz M (2003) Targets of the transcriptional repressor oncoprotein gfi-1.

- 856 Proc Natl Acad Sci U S A 100: 5932-7.
- 857 97. Chen H, Zhang P, Radomska HS, Hetherington CJ, Zhang DE, et al. (1996) Octamer  
858 binding factors and their coactivator can activate the murine pu.1 (spi-1) promoter.  
859 J Biol Chem 271: 15743-52.
- 860 98. Behre G, Whitmarsh AJ, Coghlan MP, Hoang T, Carpenter CL, et al. (1999) c-jun  
861 is a jnk-independent coactivator of the pu.1 transcription factor. J Biol Chem 274:  
862 4939-46.
- 863 99. Kardassis D, Papakosta P, Pardali K, Moustakas A (1999) c-jun transactivates the  
864 promoter of the human p21(waf1/cip1) gene by acting as a superactivator of the  
865 ubiquitous transcription factor sp1. J Biol Chem 274: 29572-81.
- 866 100. Johnson DG, Ohtani K, Nevins JR (1994) Autoregulatory control of e2f1 expression  
867 in response to positive and negative regulators of cell cycle progression. Genes Dev  
868 8: 1514-25.
- 869 101. Fu M, Zhang J, Lin Y, Zhu X, Ehrengruber MU, et al. (2002) Early growth response  
870 factor-1 is a critical transcriptional mediator of peroxisome proliferator-activated  
871 receptor-gamma 1 gene expression in human aortic smooth muscle cells. J Biol  
872 Chem 277: 26808-14.
- 873 102. Mak KS, Funnell APW, Pearson RCM, Crossley M (2011) Pu.1 and haematopoietic  
874 cell fate: Dosage matters. Int J Cell Biol 2011: 808524.
- 875 103. Chen F, Wang Q, Wang X, Studzinski GP (2004) Up-regulation of egr1 by 1,25-  
876 dihydroxyvitamin d3 contributes to increased expression of p35 activator of cyclin-  
877 dependent kinase 5 and consequent onset of the terminal phase of hl60 cell differ-  
878 entiation. Cancer Res 64: 5425-33.
- 879 104. Suh J, Jeon YJ, Kim HM, Kang JS, Kaminski NE, et al. (2002) Aryl hydrocarbon  
880 receptor-dependent inhibition of ap-1 activity by 2,3,7,8-tetrachlorodibenzo-p-dioxin  
881 in activated b cells. Toxicol Appl Pharmacol 181: 116-23.

- 882 105. Shen M, Bunaci RP, Congleton J, Jensen HA, Sayam LG, et al. (2011) Inter-  
883       feron regulatory factor-1 binds c-cbl, enhances mitogen activated protein kinase  
884       signaling and promotes retinoic acid-induced differentiation of hl-60 human myelo-  
885       monoblastic leukemia cells. *Leuk Lymphoma* 52: 2372-9.
- 886 106. Bunaci RP, Yen A (2011) Activation of the aryl hydrocarbon receptor ahr promotes  
887       retinoic acid-induced differentiation of myeloblastic leukemia cells by restricting ex-  
888       pression of the stem cell transcription factor oct4. *Cancer Res* 71: 2371-80.
- 889 107. Bock KW (2017) 2,3,7,8-tetrachlorodibenzo-p-dioxin (tcdd)-mediated deregulation  
890       of myeloid and sebaceous gland stem/progenitor cell homeostasis. *Arch Toxicol* 91:  
891       2295-2301.
- 892 108. Jackson DA, Pombo A, Iborra F (2000) The balance sheet for transcription: an anal-  
893       ysis of nuclear rna metabolism in mammalian cells. *FASEB J* 14: 242-54.
- 894 109. Zhao ZW, Roy R, Gebhardt JCM, Suter DM, Chapman AR, et al. (2014) Spatial orga-  
895       nization of rna polymerase ii inside a mammalian cell nucleus revealed by reflected  
896       light-sheet superresolution microscopy. *Proc Natl Acad Sci U S A* 111: 681-6.
- 897 110. Freitas R, Merkle R (2004) Kinematic Self-Replicating Machines. Oxford University  
898       Press.
- 899 111. Yang E, van Nimwegen E, Zavolan M, Rajewsky N, Schroeder M, et al. (2003) De-  
900       cay rates of human mrnas: correlation with functional characteristics and sequence  
901       attributes. *Genome Res* 13: 1863-72.
- 902 112. Doherty MK, Hammond DE, Clague MJ, Gaskell SJ, Beynon RJ (2009) Turnover  
903       of the human proteome: determination of protein intracellular stability by dynamic  
904       silac. *J Proteome Res* 8: 104-12.
- 905 113. Sehgal PB, Derman E, Molloy GR, Tamm I, Darnell JE (1976) 5,6-dichloro-1-beta-  
906       d-ribofuranosylbenzimidazole inhibits initiation of nuclear heterogeneous rna chains  
907       in hela cells. *Science* 194: 431-3.

- 908 114. Darzacq X, Shav-Tal Y, de Turris V, Brody Y, Shenoy SM, et al. (2007) In vivo dy-  
909 namics of rna polymerase ii transcription. *Nat Struct Mol Biol* 14: 796-806.
- 910 115. Kos M, Tollervey D (2010) Yeast pre-rrna processing and modification occur cotran-  
911 scriptionally. *Mol Cell* 37: 809-20.
- 912 116. Darnell JE Jr (2013) Reflections on the history of pre-mrna processing and highlights  
913 of current knowledge: a unified picture. *RNA* 19: 443-60.
- 914 117. Boström K, Wettsten M, Borén J, Bondjers G, Wiklund O, et al. (1986) Pulse-chase  
915 studies of the synthesis and intracellular transport of apolipoprotein b-100 in hep g2  
916 cells. *J Biol Chem* 261: 13800-6.
- 917 118. Meyers R, editor (2004) *Encyclopedia of Molecular Cell Biology and Molecular  
918 Medicine*, Volume 1, 2nd Edition. ISBN: 978-3-527-30543-8. Wiley-Blackwell.
- 919 119. Rosenbluth MJ, Lam WA, Fletcher DA (2006) Force microscopy of nonadherent  
920 cells: a comparison of leukemia cell deformability. *Biophys J* 90: 2994-3003.
- 921 120. O'Leary NA, Wright MW, Brister JR, Ciufo S, Haddad D, et al. (2016) Reference  
922 sequence (refseq) database at ncbi: current status, taxonomic expansion, and func-  
923 tional annotation. *Nucleic Acids Res* 44: D733-45.
- 924 121. Wallace AS, Supnick HT, Bunaciu RP, Yen A (2016) Rrd-251 enhances all-trans  
925 retinoic acid (ra)-induced differentiation of hl-60 myeloblastic leukemia cells. *Oncot-  
926 target* 7: 46401.
- 927 122. Congleton J, MacDonald R, Yen A (2012) Src inhibitors, pp2 and dasatinib, in-  
928 crease retinoic acid-induced association of lyn and c-raf (s259) and enhance mapk-  
929 dependent differentiation of myeloid leukemia cells. *Leukemia* 26: 1180–1188.
- 930 123. Congleton J, Shen M, MacDonald R, Malavasi F, Yen A (2014) Phosphorylation of  
931 c-cbl and p85 pi3k driven by all-trans retinoic acid and cd38 depends on lyn kinase  
932 activity. *Cellular signalling* 26: 1589–1597.
- 933 124. Bunaciu RP, Jensen HA, MacDonald RJ, LaTocha DH, Varner JD, et al. (2015)

- 934 6-formylindolo(3,2-b)carbazole (ficz) modulates the signalsome responsible for  
935 ra-induced differentiation of hl-60 myeloblastic leukemia cells. PLoS One 10:  
936 e0135668.
- 937 125. Shen M, Yen A (2008) c-cbl interacts with cd38 and promotes retinoic acid–induced  
938 differentiation and g0 arrest of human myeloblastic leukemia cells. Cancer research  
939 68: 8761–8769.

**Table 1:** Myelomonocytic transcription factor connectivity used in the signal integration and phenotype modules.

Effector	Effect	Target	Source
RAR $\alpha$	+	RAR $\alpha$	(64)
	+	PU.1	(65)
	+	C/EBP $\alpha$	(42)
	+	IRF-1	(66)
	-	Oct4	(67)
	+	CD38	(68)
	+	p21	(69)
	+	AhR	(70)
	+	Egr-1	(71)
PPAR $\gamma$	+	C/EBP $\alpha$	(72)
	+	IRF-1	(73)
	+	Oct1	(74)
	-	AP-1	(75)
	-	E2F	(76)
	-	Egr-1	(77)
	+	CD38	(78)
	+	CD14	(79)
	+	p21	(80)
	-	p47Phox	(81)
PU.1	-	PPAR $\gamma$	(82)
	+	PU.1	(83)
	+	AP-1	(84)
	+	Egr-1	(38)
	+	CD11b	(85)
	+	p21	(86)
	+	p47Phox	(87)
C/EBP $\alpha$	+	PPAR $\gamma$	(72)
	+	PU.1	(43)
	+	C/EBP $\alpha$	(88)
	+	Gfi-1	(89)
	-	E2F	(90)
	+	CD14	(91)

941

	+	p21	(92)
IRF-1	+	CD38	(93)
	+	p21	(94)
	-	PU.1	(95)
	-	C/EBP $\alpha$	(96)
	-	E2F	(96)
	-	Egr-1	(38)
	-	p21	(96)
Oct1	+	PU.1	(97)
AP-1	-	PPAR $\gamma$	(75)
	+	PU.1	(98)
	+	p21	(99)
E2F	+	E2F	(100)
Egr-1	+	PPAR $\gamma$	(101)
	-	Gfi-1	(102)
	+	CD14	(103)
AhR	+	AP-1	(104)
	+	IRF-1	(105)
	-	Oct4	(106)
	-	PU.1	(107)

**Table 2:** Characteristic model parameters estimated from literature.

Symbol	Description	Value	Units	Source
$R_1$	RNA polymerase abundance	85,000	copies/cell	(108, 109)
$R_2$	Ribosome abundance	$1 \times 10^6$	copies/cell	(110)
$G_i$	Characteristic gene abundance	2	copies/cell	this study
$K_X$	Saturation constant transcription	600	copies/cell	this study
$K_T$	Saturation constant translation	95,000	copies/cell	this study
$t_{1/2,m}$	characteristic mRNA half-life (transcription factor)	2-4	hr	(111)
$t_{1/2,p}$	characteristic protein half-life	10	hr	(112)
$\theta_{m,j}$	characteristic mRNA degradation constant	0.34	$hr^{-1}$	derived
$\theta_{p,j}$	characteristic protein degradation constant	0.07	$hr^{-1}$	derived
944	$t_d$	HL-60 doubling time	19.5	hr
	$\mu$	growth rate	0.035	$hr^{-1}$
	$k_d$	death rate	$0.10\mu$	$hr^{-1}$
	$e_T$	elongation rate RNA polymerase	50-100	nt/s
	$e_X$	elongation rate Ribosome	5	aa/s
	$L_{T,o}$	characteristic gene length	44,192	nt
	$L_{X,o}$	characteristic transcript length	1,374	nt
	$k_T$	characteristic transcription rate	1.44	$hr^{-1}$
	$k_X$	characteristic translation rate	3.60	$hr^{-1}$
	$D$	Diameter of an HL-60 cell	12.4	$\mu m^3$
	$f_C$	cytoplasmic fraction	0.51	dimensionless

945 **Table 3:** Sequence lengths from NCBI RefSeq database were used in the signal integration and phenotype  
 946 modules (120). The RNA sequence length used represents the total distance of transcription, and assume  
 to be equal to the gene length.

Gene Name	Gene (bp)	RNA (bp)	Protein (aa)	Gene ID	Protein ID
AP-1	10323	10323	331	Gene ID: 3725	NP_002219
AhR	47530	47530	848	Gene ID: 196	NP_001621
CD11b	72925	72925	1153	Gene ID: 3684	NP_001139280
CD14	8974	8974	375	Gene ID: 929	NP_001035110
CD38	174978	74978	300	Gene ID: 952	NP_001766
C/EBP $\alpha$	2630	2630	393	Gene ID: 1050	NP_001274353.1
E2F	17919	17919	437	Gene ID: 1869	NP_005216
Egr-1	10824	10824	543	Gene ID: 1958	NP_001955
Gfi-1	13833	13833	422	Gene ID: 2672	NP_005254
IRF-1	16165	16165	325	Gene ID: 3659	NP_002189
Oct1	206516	206516	741.33	Gene ID: 5451	NP_002688.3, NP_001185712.1, NP_001185715.1
Oct4	6356	6356	206.33	Gene ID: 5460	NP_001167002, NP_001167015, NP_001167016
P21	15651	15651	198	NG_009364.1	NP_001621
P47	3074	3074	390	GenBank: AF003533.1	NP_000256
PPAR $\gamma$	153507	153507	250	Gene ID: 5468	NP_001317544
PU.1	40782	40782	270.5	Gene ID: 6688	NP_001074016, NP_003111

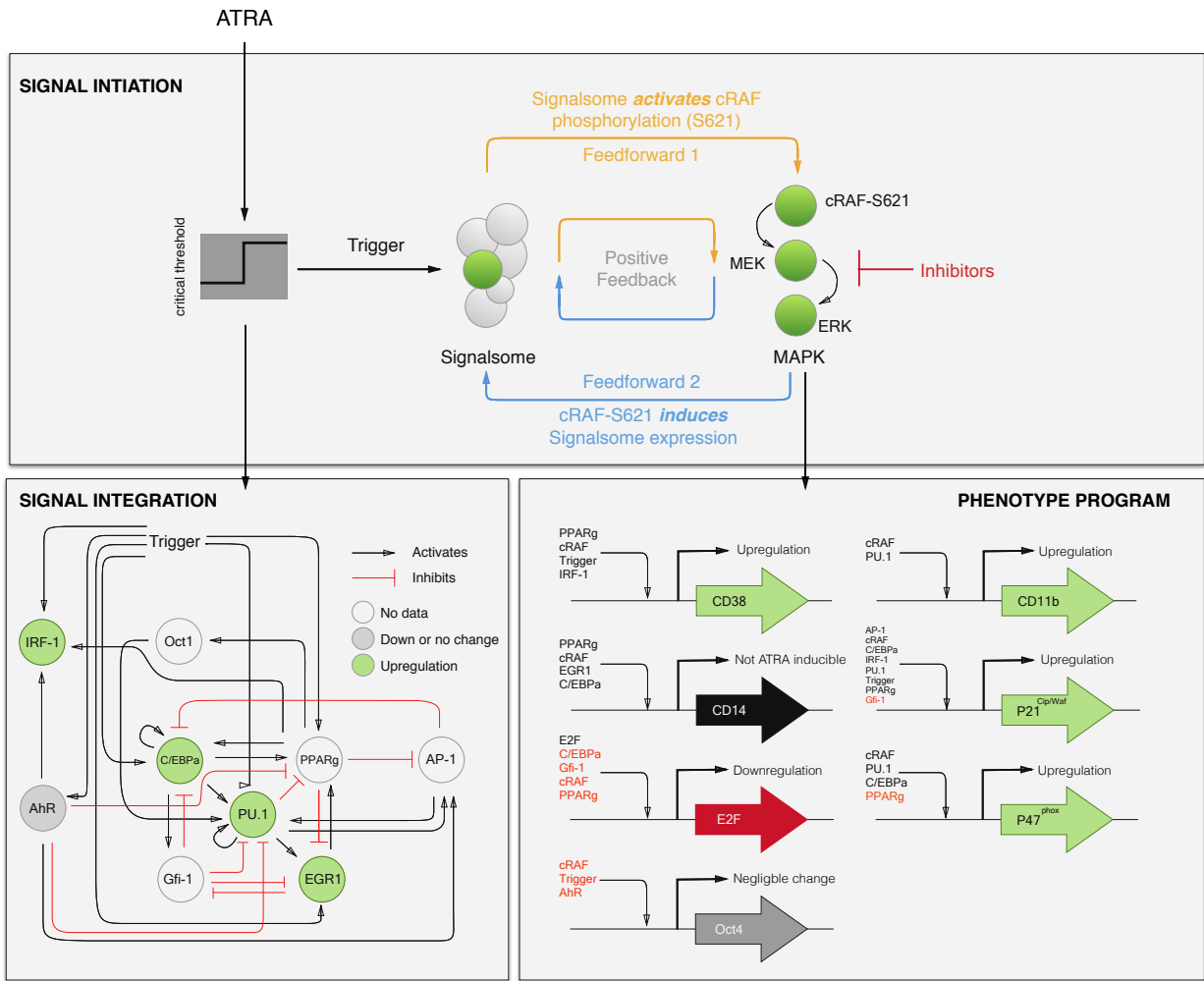


**Fig. 1:** Schematic of the effective ATRA differentiation circuit. Above a critical threshold, ATRA activates an upstream Trigger, which induces signalsome complex formation. Signalsome activates the mitogen-activated protein kinase (MAPK) cascade which in turn drives the differentiation program and signalsome formation. Both Trigger and activated cRaf-pS621 drive a phenotype gene expression program responsible for differentiation. Trigger activates the expression of a series of transcription factors which in combination with cRaf-pS621 result in phenotypic change.

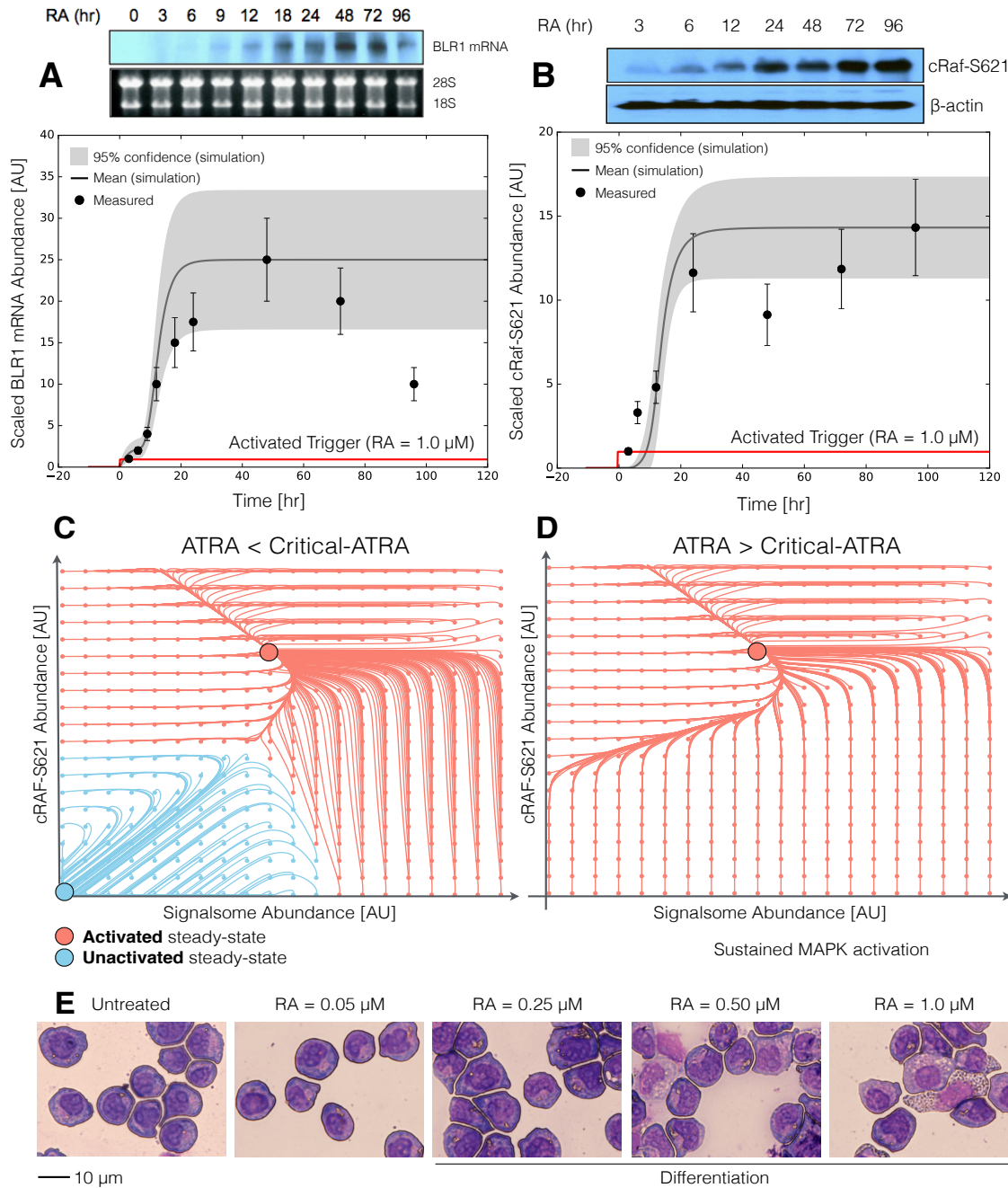


**Fig. 2:** Model analysis for ATRA-induced HL-60 differentiation. A: BLR1 mRNA versus time following exposure to 1  $\mu$ M ATRA at t = 0 hr. B: cRaf-pS621 versus time following exposure to 1  $\mu$ M ATRA at t = 0 hr. Points denote experimental measurements, solid lines denote the mean model performance. Shaded regions denote the 99% confidence interval calculated over the parameter ensemble. C: Signalsome and cRaf-pS621 nullclines for ATRA below the critical threshold. The model had two stable steady states and a single unstable state in this regime. D: Signalsome and cRaf-pS621 nullclines for ATRA above the critical threshold. In this regime the model had only a single stable steady state. E: Morphology of HL-60 as a function of ATRA concentration (t = 72 hr).

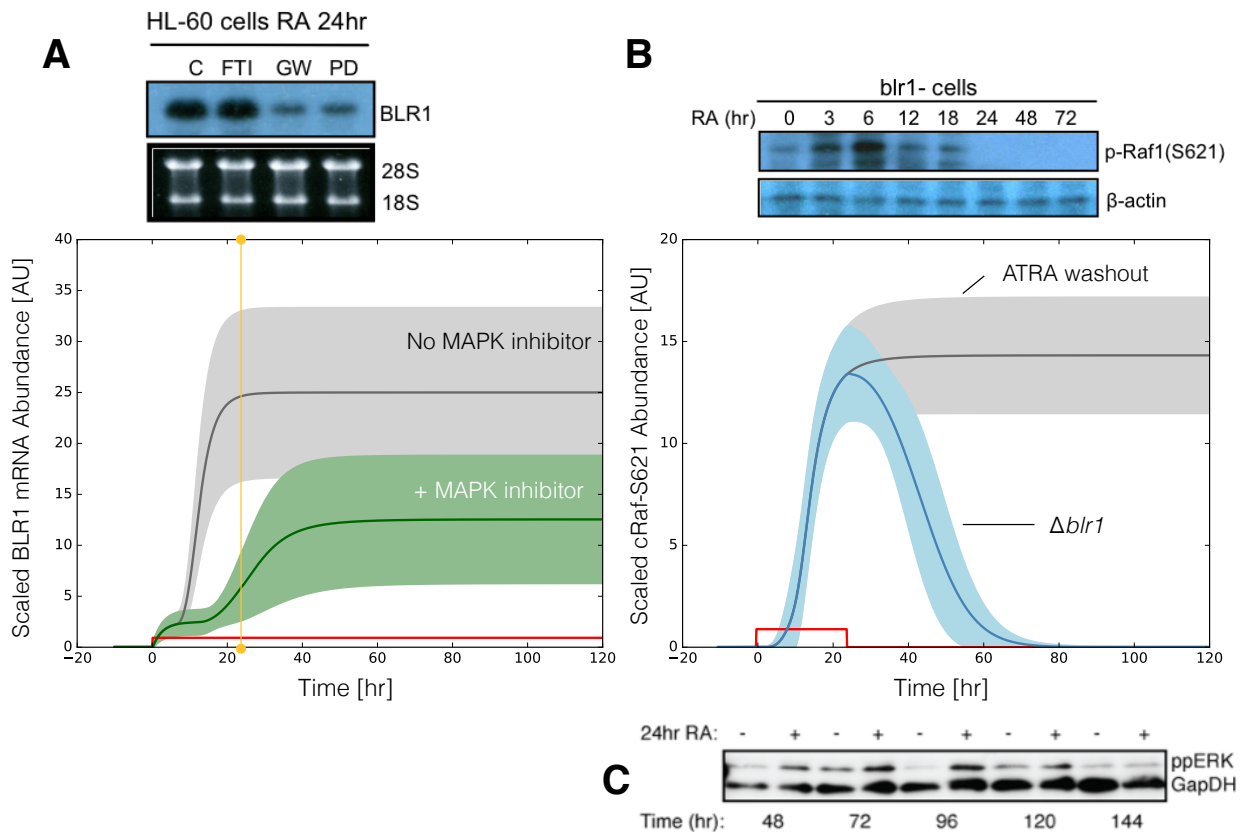


**Fig. 3:** Model simulation following exposure to  $1\mu\text{M}$  ATRA. A: BLR1 mRNA versus time with and without MAPK inhibitor. B: cRaf-pS621 versus time following pulsed exposure to  $1\mu\text{M}$  ATRA with and without BLR1. Solid lines denote the mean model performance, while shaded regions denote the 99% confidence interval calculated over the parameter ensemble. C: Western blot analysis of phosphorylated ERK1/2 in ATRA washout experiments. Experimental data in panels A and B were reproduced from Wang and Yen (25), data in panel C is reported in this study.

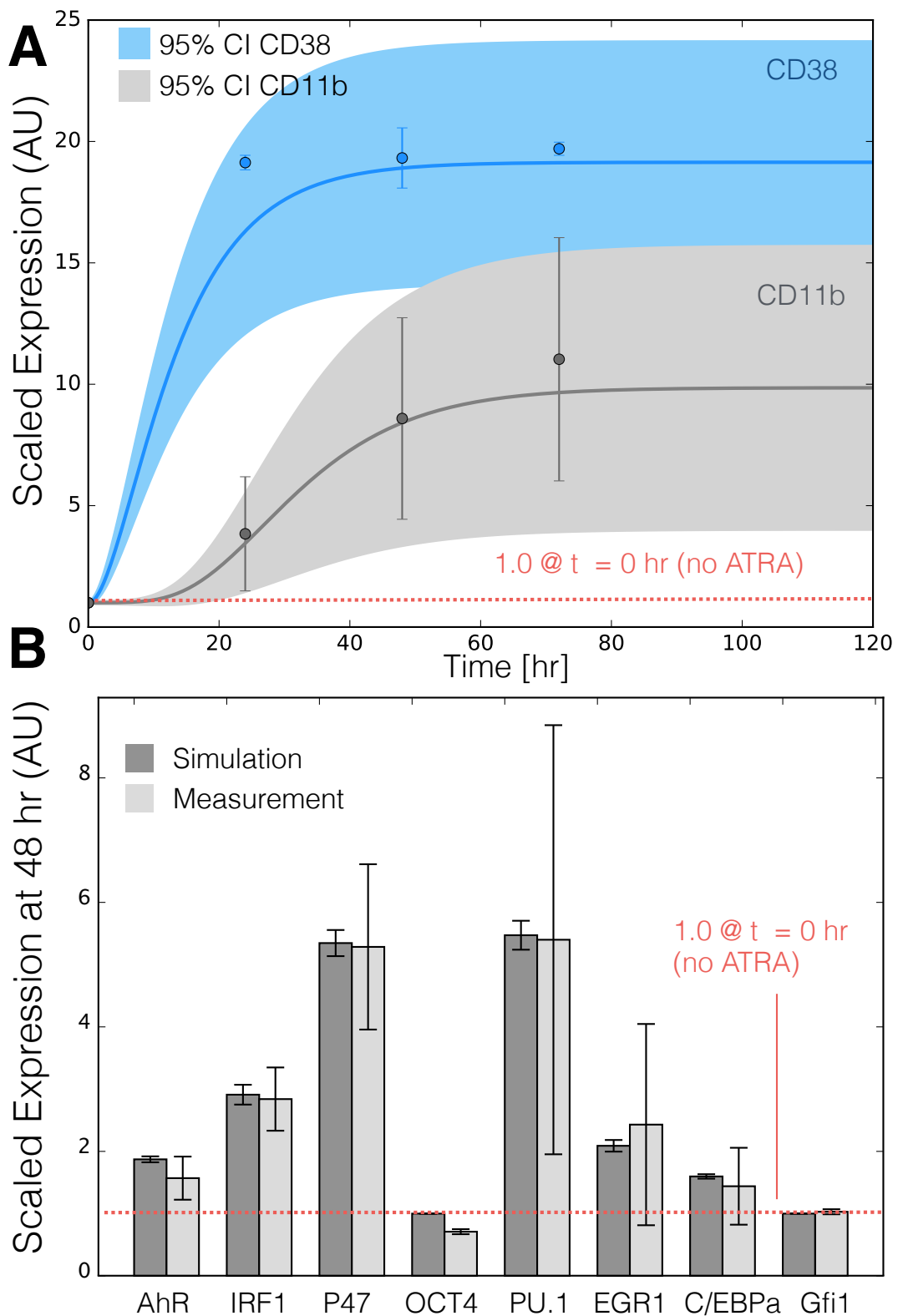


**Fig. 4:** Model simulation of the HL-60 gene expression program following exposure to  $1\mu\text{M}$  ATRA at  $t = 0$  hr. A: CD38 and CD11b expression versus time following ATRA exposure at time  $t = 0$  hr. B: Gene expression at  $t = 48$  hr following ATRA exposure. Experimental data in panels A and B were reproduced from Jensen et al. (31).

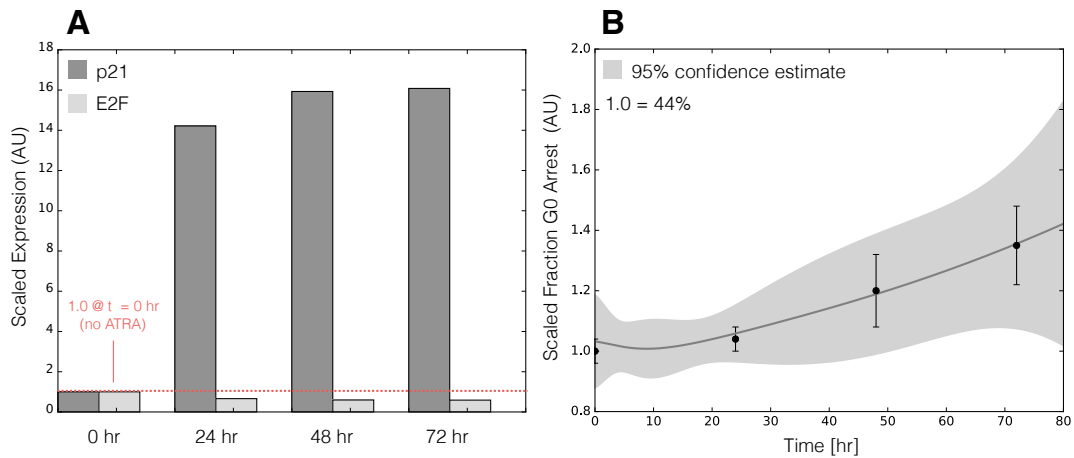


**Fig. 5:** Model simulation of HL-60 cell-cycle arrest following exposure to  $1\mu\text{M}$  ATRA at  $t = 0$  hr. A: Predicted p21 and E2F expression levels for the best parameter set following ATRA exposure at time  $t = 0$  hr. B: Estimated fraction of HL-60 cells in G0 arrest following ATRA exposure at time  $t = 0$  hr. The gray region denotes the 95% confidence estimate of the polynomial model. Experimental data in panel B was reproduced from Jensen et al. (31).

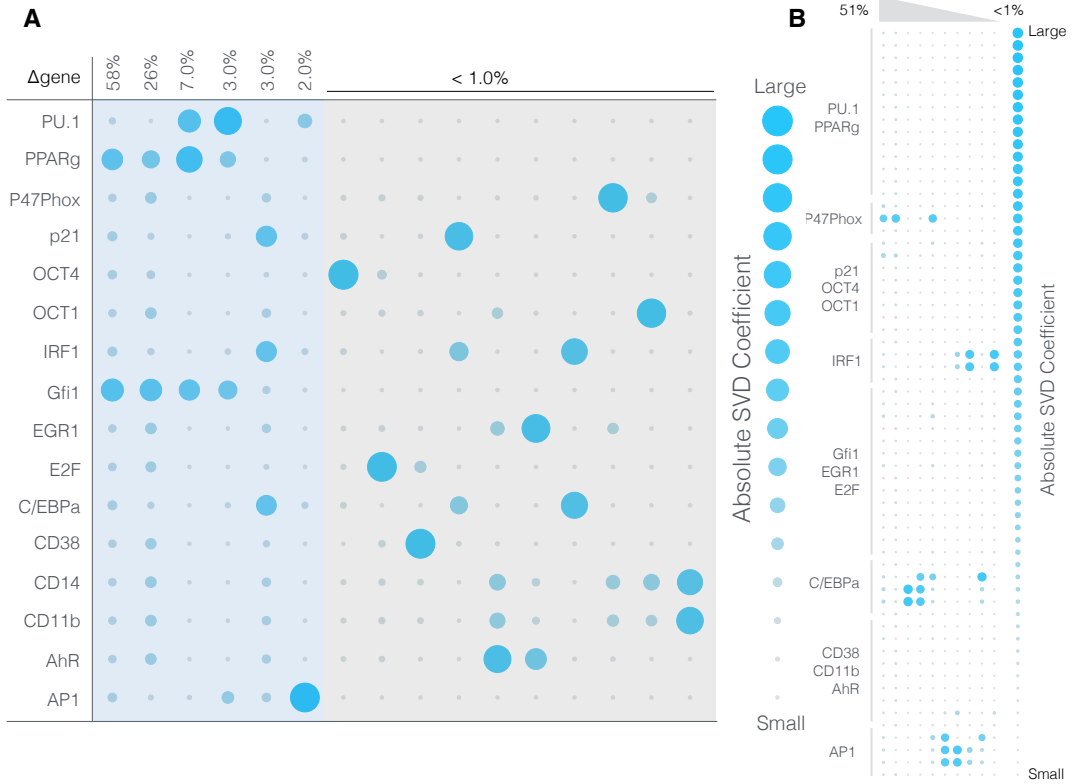


**Fig. 6:** Robustness of the HL-60 differentiation program following exposure to  $1\mu\text{M}$  ATRA at  $t = 0$  hr. A: Singular value decomposition of the system response ( $l^2$ -norm between the perturbed and nominal state) following pairwise gene knockout simulations using the best fit parameter set. The percentage at the top of each column describes the fraction of the variance in the system state captured by the node combinations in the rows. B: Singular value decomposition of the system response ( $l^2$ -norm between the perturbed and nominal state) following the pairwise removal of connections.

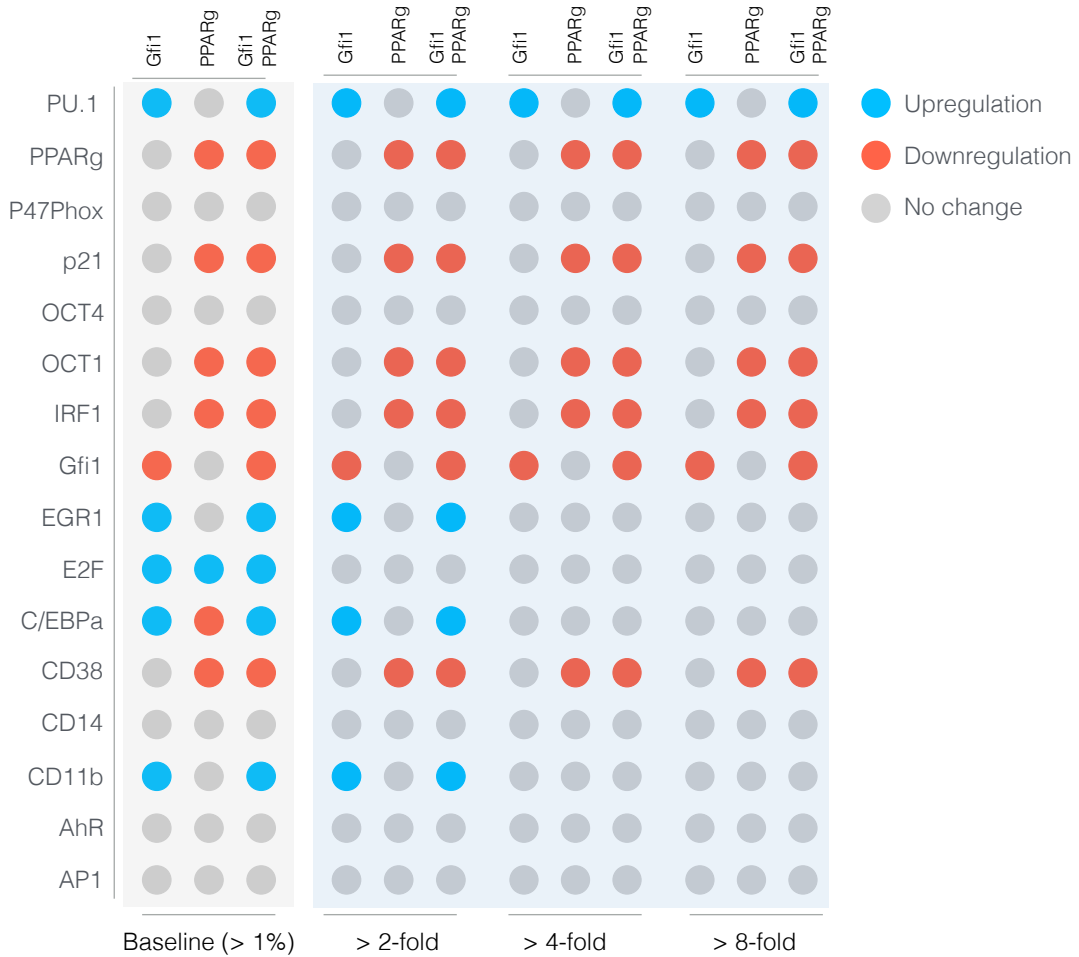


**Fig. 7:** Robustness of the HL-60 differentiation program following exposure to  $1\mu\text{M}$  ATRA at  $t = 0$  hr. Protein fold change at  $t = 48$  hr (rows) in single and double knock-out mutants (columns) relative to wild-type HL-60 cells. The responses were grouped into  $>2,4$  and  $8$  fold changes. The best fit parameter set was used to calculate the protein fold change.

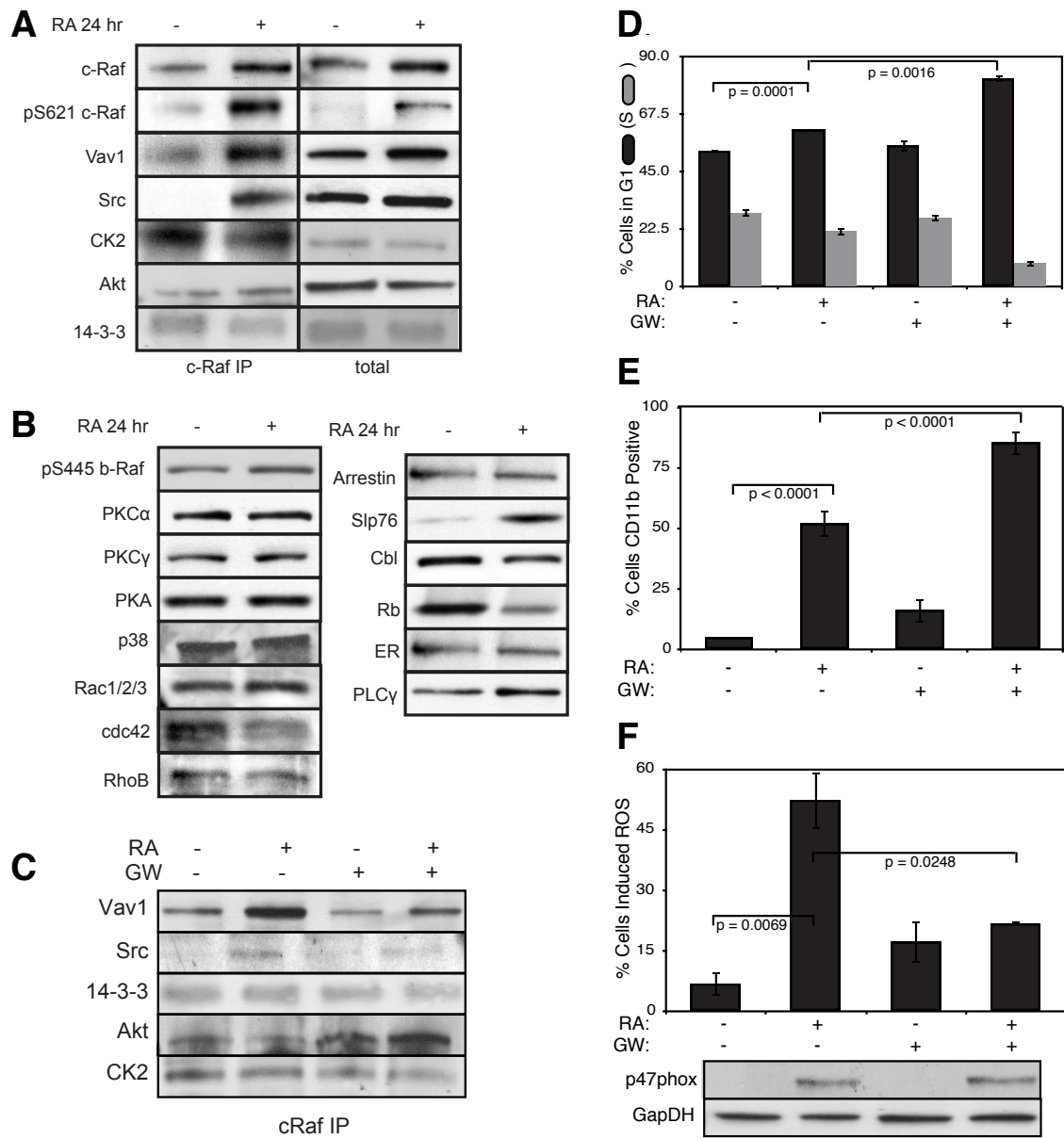


**Fig. 8:** Investigation of a panel of possible Raf interaction partners in the presence and absence of ATRA. A: Species identified to precipitate out with Raf: first column shows Western blot analysis on total Raf immunoprecipitation with and without 24 hr ATRA treatment and the second on total lysate. B: The expression of species considered that did not precipitate out with Raf at levels detectable by Western blot analysis on total lysate. C: Effect of the Raf inhibitor GW5074 on Raf interactions as determined by Western blot analysis of total Raf immunoprecipitation. The Authors note the signal associated with Src was found to be weak. D: Cell Cycle distribution as determined by flow cytometry indicated arrest induced by ATRA, which was increased by the addition of GW5074. E: Expression of the cell surface marker CD11b as determined by flow cytometry indicated increased expression induced by ATRA, which was enhanced by the addition of GW5074. F: Inducible reactive oxygen species (ROS) as determined by DCF flow cytometry. The functional differentiation response of ATRA treated cells was mitigated by GW5074.

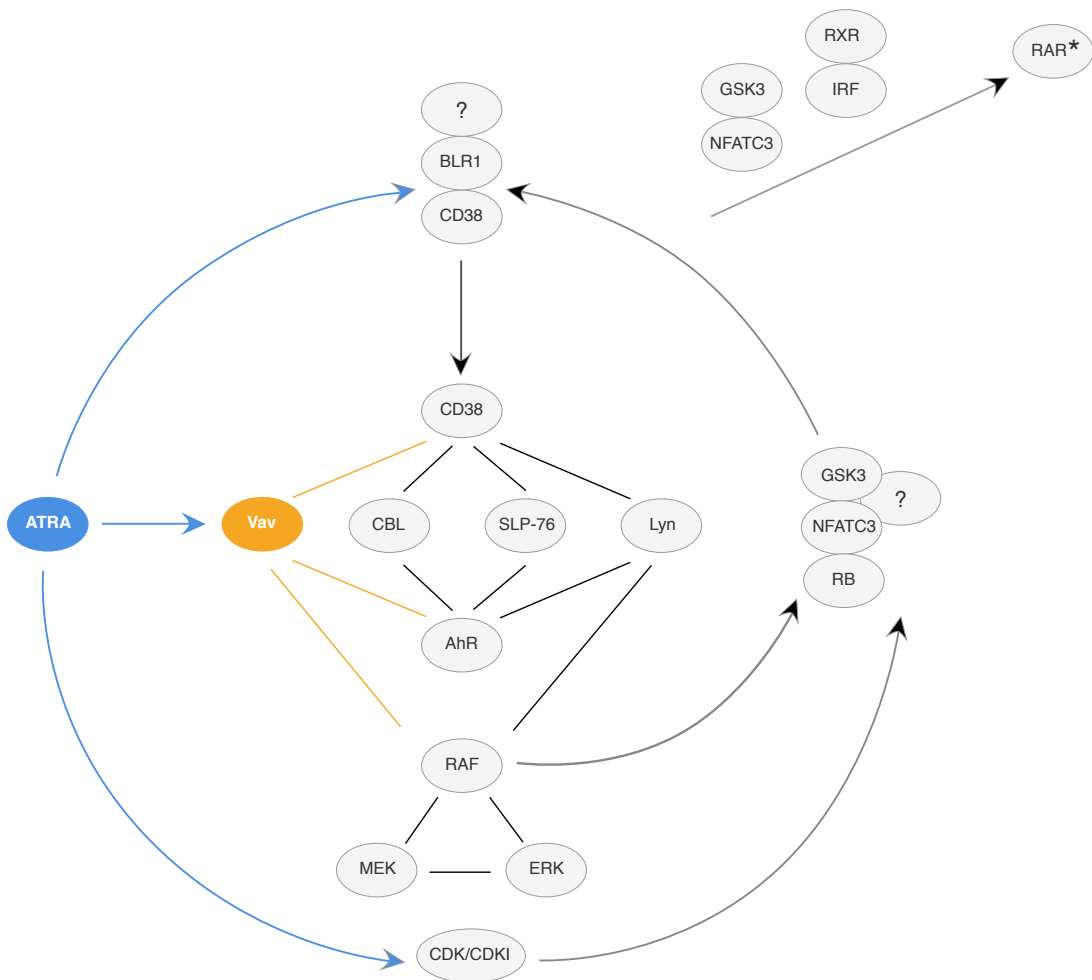


**Fig. 9:** Schematic of the hypothetical principal pathways in the ATRA-induced signaling that results in cell differentiation in the HL-60 myeloid leukemia model (17, 121–125). It is based on modules and feedback loops. There are three main arms (shown top to bottom): 1. Direct ATRA targeting of RAREs in genes such as CD38 or BLR1; 2. Formation of a signalsome that has a regulatory module that includes Vav (a GEF), CBL and SLP-76 (adaptors), and Lyn (a SFK) that regulates a Raf/Mek/Erk axis that incorporates Erk to Raf feedback, where the regulators are modulated by AhR and CD38 receptors; and 3. Direct ATRA targeted up regulation of CDKI to control RB hypophosphorylation. The Raf/Mek/Erk axis is embedded in the signalsome and subject to modulation by the regulators. The output of the signalsome is discharge of the Raf from the cytosol to the nucleus where it binds (hyper)phospho-RB and other targets, including NFATc3, which enables activation of the RA bound RAR/RXR poised on the BLR1 promoter, and also GSK3, phosphorylation of which relieves its inhibitory effect on RAR $\alpha$ . CDKI directed hypophosphorylation of RB releases Raf sequestered by RB to go to NFATc3, GSK3, and other targets. A significant consequence of the nuclear RAF is ergo ultimately to hyperactivate transcriptional activation by RAR $\alpha$  to drive differentiation. It might be noted that this general proposed model provides a mechanistic rationalization for why cell cycle arrest is historically oft times perceived as a feature predisposing phenotypic maturation.